Journal of Industrial and Engineering Chemistry xxx (xxxx) xxx

Contents lists available at ScienceDirect

Journal of Industrial and Engineering Chemistry

journal homepage: www.elsevier.com/locate/jiec

Feasibility analysis and mechanism study of different sulfate waste residues for carbothermal reduction of phosphorite in a fluidized bed

Zhihua Tian [1], Bin Zhang [1], Jiahe Yue [1], Qinhui Wang [*]

State Key Laboratory of Clean Energy Utilization, Zhejiang University, Hangzhou 310027, China

ARTICLE INFO

Keywords:
Fluidized bed
Thermal reduction
Phosphorite
Coal
Sulfates

ABSTRACT

The thermal reduction of phosphorite offers high product purity and no by-products but is limited by high costs. Traditional methods that utilize fixed beds and kilns challenges like high reaction temperatures, extended processing durations, and substantial costs. Meanwhile, managing sulfate-based industrial waste, rich in silica and sulfate, remains unresolved. This study employs a fluidized bed reactor for phosphorite reduction and explores the use of sulfate-based wastes as an additive. By adding four sulfate additives in phosphorite, the study improves the conversion ratio of phosphorite and presents a cost-effective solution for waste management. Optimal operational parameters were determined, and the impact of additives and pretreatment on the reduction process was analyzed. Results indicate that sulfate additives increase the conversion ratio by 10 %-15 %, with pretreatment providing an additional 5 %–10 % improvement.

Introduction

Phosphorite, a critical mineral resource, is vital for producing yellow phosphorus and phosphoric acid, with China supplying approximately 40 % of global reserves [1,2]. The increasing demand for high-purity phosphoric acid in agriculture, pharmaceuticals, and other industries highlights the importance of efficient resource utilization [3,4]. Currently, phosphoric acid is produced via the wet or thermal process [5]. While the wet process is cost-effective and achieves a high conversion ratio [6], it requires high-grade phosphorite and produces low-purity products alongside environmentally challenging by-products like phosphogypsum [7]. The reactors used in the thermal reduction process of phosphorite mainly include fixed beds and kilns. The fixed-bed reactor requires an optimal temperature above 1300 °C and a reduction time exceeding 1 h, resulting in an industrial production conversion ratio typically around 50 % with high production costs [8,9]. Although the kiln method achieves an optimal temperature range of 1250–1300 °C for phosphorite reduction, yielding a conversion ratio of approximately 70 %, its process is hindered by prolonged reaction times and current technical constraints, preventing industrialization [10]. Conversely, the thermal process can utilize low- and medium-grade phosphorite to produce high-purity phosphoric acid but is cost-intensive due to high reaction temperatures and energy requirements [11,12].

To tackle the challenges in the thermal process, researchers have focused on improving thermal phosphoric acid technology and optimizing phosphorite reduction processes [13–18]. Li et al. [19] elucidated the optimal process parameters for phosphorite reduction within the electric furnace. Jiang [20] systematically evaluated the influence of various factors on the reduction of phosphorite. Hu [21] found that graphite powder demonstrated superior reducibility relative to coke. Lan [22] found that the incorporation of a well-balanced mixture of SiO_2,MgO, and Al_2O_3 in appropriate proportions could substantially decrease the melting point of phosphorite. Luo [23] studied the impact of various sources of silicon on the reaction. The findings revealed their promotion effect in the following descending order: potassium silicate > sodium silicate > fly ash > silica dioxide. Cao et al. [10], using kiln reduction of phosphorite, found that K_2CO_3, Na_2CO_3, $NiSO_4$, and K_2CO_3-$NiSO_4$ compounds, as additives, effectively heightened the reactivity of coal, then reduced the reaction activation energy, consequently leading to an elevated phosphorite conversion ratio. In summary, numerous scholars have carried out extensive studies focusing on the optimization of the phosphorite reduction process. These studies have explored the influence and effects of process parameters, influencing factors, reducing agents, additives on thermal phosphorite reduction.

Despite these advancements, limited studies have explored the use of

* Corresponding author.
E-mail address: qhwang@zju.edu.cn (Q. Wang).
[1] These authors contributed equally to this work.

https://doi.org/10.1016/j.jiec.2025.03.030
Received 15 January 2025; Received in revised form 1 March 2025; Accepted 12 March 2025
Available online 14 March 2025

fluidized beds for phosphorite reduction, and none have investigated the addition of sulfate to enhance the thermal reduction process. The novelty of this study lies in the employment of the fluidized bed reactor for the reduction of phosphorite, along with the exploration of the feasibility of using sulfate industrial waste as an additive for thermal reduction of phosphorite. The amount of sulfate industrial waste generated each year is huge, which takes a lot of manpower and financial resources to deal with it. Therefore, this study proposes an innovative approach to utilize these waste materials effectively. Silicon dioxide in the waste serves as a necessary reactant for phosphorite reduction, while sulfate compounds act as additives to enhance the carbothermal reduction of fluorapatite in phosphorite, boosting conversion ratio. This study investigated the feasibility of this process by conducting experiments using four sulfate salts in a fluidized bed reactor. This research aims to improve phosphorite conversion ratios, minimize costs, and explore sustainable solutions for repurposing sulfate industrial waste, contributing to both resource efficiency and environmental sustainability.

Experimental

Materials

To validate the universality of the conclusions obtained, three types of Yunnan phosphorite with varying compositions were selected for experimental verification. As shown in Table 1, the fluorine content in the three types of phosphorite is relatively high, suggesting that the phosphorus in these phosphorites mainly exists in the form of calcium fluorophosphate. The P_2O_5 mass fractions in these three phosphorites are 24.82 %, 22.29 %, and 19.66 %, respectively. These all belong to low- and medium-grade phosphorite, and the composition of these phosphorites is shown in Table 1. In these experiments, high ash point Hua Dian coal served as the designated reducing agent, and the analytical findings pertaining to its industrial, elemental, and calorific characteristics are outlined in Table 2. Additionally, SiO_2 and other inorganic additives used in these experiments were all analytical-grade reagents.

Due to the utilization of a fluidized bed reactor, the materials should not clog or slag at high reaction temperature. So, it becomes essential to conduct an analysis of the ash melting point of the raw materials prior to this experiment. Ash melting point tests were performed on three phosphorites and Huadian coal. It can be seen from Table 3, the softening temperature of the phosphorite was low. Therefore, for this experiment, it was crucial to ensure that the maximum reaction temperature could not exceed 1300 °C to prevent softening or melting of the phosphorite.

Since the reactor used in this experiment is a fluidized bed, the properties of the particles will affect the fluidization effect. Table 4 shows the particle size, density and Geldart classification of the particles used in this research. Most of the particles selected in this experiment are Class B particles. This shows that the sample can be fluidized relatively easily in the fluidized bed without the need for excessively high gas velocity or special fluidization auxiliary means. This is more advantageous for using a fluidized bed for thermal reduction of phosphorite, and can ensure operational efficiency and stability.

Experimental setup

In the present experimental setup, a bubbling fluidized bed reactor was utilized, as shown in Fig. 1. The furnace tube and the air distribution plate were both fabricated from corundum. The corundum tube exhibited an inner diameter of 40 mm, an outer diameter of 50 mm, and a height of 120 mm. Nitrogen served as the carrier gas in this experiment. In each experimental run, 15 g of phosphorite with a particle size ranging from 0.075 to 0.150 mm was introduced, which corresponded to a bed height of 37 mm. The heating zone was furnished with silicon molybdenum rods for electric heating and was capable of reaching a maximum temperature of 1673 K.

In order to make the particles appear suspended or fluidized so that the materials can fully contact and react, it is necessary to first measure the U_{mf} (minimum fluidization velocity) of the carrier gas for the particles in a fluidized bed. The U_{mf} refers to the minimum airflow velocity in the gas–solid fluidized bed system when the airflow velocity gradually increases and the solid particles begin to change from a static accumulation state to a fluidized state. It is a key parameter in the operation of the fluidized bed and plays a decisive role in the stability and reaction effect of the entire fluidization process. This research adopts the approach prevalently utilized in prior investigations [24–26] to gauge the correlation between the pressure drop and velocity of gas within a fluidized bed, thereby ascertaining the U_{mf}. When the velocity of gas traversing the bed is extremely low, the bed pressure drop escalates in direct proportion to the augmentation of the velocity of gas. As the velocity of gas ascends to a constant value, the bed pressure drop attains the maximum value $\triangle P_{max}$, which is marginally higher than the static pressure of the entire bed. If the gas velocity persists in increasing, the pressure will abruptly "unlock." When the velocity of gas surpasses the U_{mf}, the bed will expand and generate bubbles. Simultaneously, within a specific range of continuous velocity of gas increment, the bed pressure drop remains stable. The velocity of gas corresponding to the unlocking point is the U_{mf} of the carrier gas. The U_{mf} of the carrier gas in a fluidized bed employed in this study is 0.07 $m \bullet s^{-1}$, as measured by the cold state experiment. For the fluidized bed under actual operating circumstances, in the majority of cases, to accomplish full fluidization of the bed, the U_{op} is typically around 1.5–2 times the U_{mf} [27,28]. Taking 1.5 times the U_{mf} into account, the U_{op} (operating fluidization velocity) of the carrier gas is fixed at 0.11 $m \bullet s^{-1}$.

Methods

First of all, the raw materials, including phosphorite, SiO_2, and Hua Dian coal, were positioned in an oven and dehydrated at 105 °C ±5 °C for a duration of 5 h. Afterward, the treated materials were pulverized into fine particles with sizes spanning from 0.075 mm to 0.150 mm, rendering them prepared and suitable for utilization. For each set of experiments, 15 g of phosphorite was precisely measured. Thereafter, SiO_2, coal, and sulfate were weighed in accordance with the mass of the phosphorite specimen. The quantified components were meticulously combined and ensured a thorough and homogeneous mixture in preparation for the experiments. Once the temperature of a fluidized bed attained the pre-established value, the samples were introduced into a fluidized bed. After the reaction concluded and a fluidized bed cooled naturally, the residual slag was amassed, weighed, and then submitted to chemical analysis.

Due to the characteristics of raw materials, excessively high

Table 1
Composition of phosphorite from Yunnan.

Sample	Composition	SiO_2	Al_2O_3	Fe_2O_3	CaO	MgO	K_2O	Na_2O	P_2O_5	F
1	wt.%	21.52	1.96	1.49	28.05	17.58	0.74	0.16	24.82	3.68
2	wt.%	37.52	3.05	1.74	22.52	5.21	3.25	1.36	22.29	3.05
3	wt.%	27.27	1.85	1.22	31.36	15.00	0.60	0.16	19.66	2.88

Table 2
Industrial, elemental and calorific value analysis of coal.

Industrial wt.%			Elemental wt.%					Calorific value (MJ•kg^{-1})
A_{db}	V_{db}	FC_{db}	C_{db}	H_{db}	N_{db}	S_{db}	O_{db}	
21.83	27.97	50.2	60.47	3.73	1.08	0.41	12.48	23.29

Table 3
Ash melting characteristic temperature of phosphorite and coal.

Sample	Deformation temperature (°C)	Softening temperature (°C)	Hemispheric temperature (°C)	Flow temperature (°C)
Phosphorite 1#	1337	1362	1388	1429
Phosphorite 2#	1342	1372	1396	1437
Phosphorite 3#	1308	1354	1371	1398
Huadian Coal	>1500	>1500	>1500	>1500

Table 4
Particle size, density and Geldart classification of the sample.

Sample	Particle size (mm)	Density (g·cm^{-3})	Geldart classification
Phosphorite 1#	0.075–0.150	2.88	B
Phosphorite 2#	0.075–0.150	2.91	B
Phosphorite 3#	0.075–0.150	2.95	B
SiO_2	0.075–0.150	2.66	B
Huadian Coal	0.075–0.150	1.46	A
Aluminum sulfate	0.075–0.150	2.67	B
Magnesium sulfate	0.075–0.150	2.65	B
Sodium sulfate	0.075–0.150	2.69	B
Potassium sulfate	0.075–0.150	2.66	B

temperatures can cause the phosphorite to melt and form slag, which has the potential to disrupt the regular operation of a bubbling fluidized bed and lower the phosphorite conversion ratio. Considering the results of ash melting characteristic temperature test for the phosphorite and coal, the highest reaction temperature selected for this experiment does not exceed 1300 °C.

The contents of P_2O_5 in the collected residue and phosphorite were determined through the volumetric approach in accordance with the national standard GB/T 1871.1-1995. The calculation formula for the phosphorite conversion ratio in a bubbling fluidized bed was presented as follows.

$$\alpha = \frac{m_1 x_1 - m_2 x_2}{m_1 x_1} \times 100\% \quad (1)$$

In this formula, m_1 represents the phosphorite mass, m_2 represents the residue mass, x_1 represents the P_2O_5 mass fraction in the phosphorite, x_2 represents the P_2O_5 mass fraction in the residue, α is the phosphorite conversion ratio.

Characterization methods

The samples collected at the end of the experiment were processed and characterized. The characterization methods used include thermogravimetric, XRD, SEM-EDS.

For thermogravimetric experiments, the samples were mixed by mechanical stirring, weighed at approximately 10 mg. A temperature elevation regimen was implemented, ranging from 30 °C to 1000 °C at a rate of 10 °C/min, with purging performed using 50 mL/min of nitrogen.

An X-ray diffractometer, Japan Rigaku SmartLab SE, was selected for X-ray diffraction (XRD) testing of the samples. The instrumental parameters are as follows: The Cu target was operated at 40 kV, accompanied by a continuous scanning rate of 1°•min^{-1} and a scanning scope of 10°–80°.

A German ZEISS Sigma 300 scanning electron microscope integrated with energy-dispersive X-ray spectroscopy (SEM-EDS) was employed to dissect the micro-morphology of the samples and the relative elemental compositional distribution.

Molecular dynamics calculations

In order to better understand the intrinsic mechanism of the four sulfates on phosphorite reduction, this study used molecular dynamics simulation to calculate the adsorption properties of the four sulfates and calcium fluorophosphate. DFT calculations were performed by using the Vienna Ab-initio Simulation Package [29,30]. The exchange–correlation interactions were described by generalized gradient approximation [30] with the Perdew-Burke-Ernzerhof functional [31]. Spin-polarization was included in all the calculations and a damped van der Waals correction was incorporated using scheme of Grimme to better describe the non-bonding interactions [32]. The cut-off energies for plane waves were set to be 500 eV, and the residual force and energy on each atom during structure relaxation were converged to 0.005 eV•Å^{-1} and 10^{-5} eV,

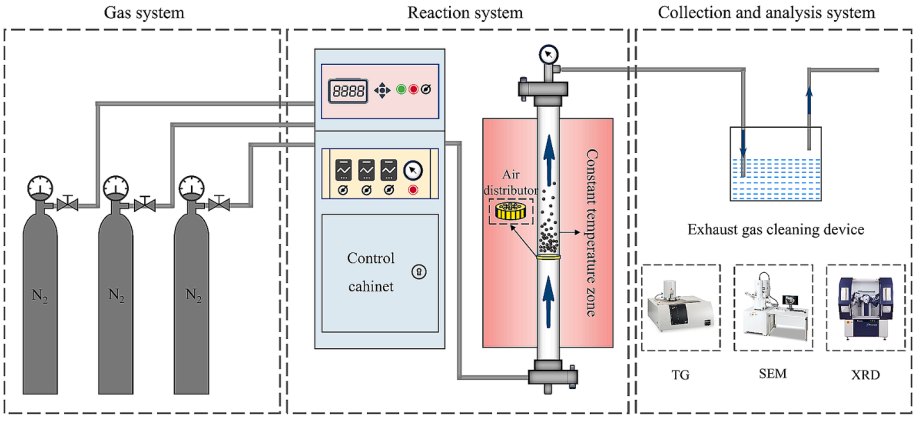

Fig. 1. Experimental equipment of a fluidized bed.

respectively. In this experiment, apatite was selected for simulation. According to previous studies [33] and XRD analysis, it can be found that slab of apatite (3 0 0) has high surface energy and reaction activity, so this study selected it for simulation. The adsorption energies (E_{ad}) for $Al_2(SO_4)_3$, $MgSO_4$, Na_2SO_4, and K_2SO_4 adsorbed on the apatite (3 0 0) are defined as $E_{ad} = E(slab + MSO_4) - E(MSO_4) - E(slab)$, Where E(slab + MSO_4) is the total energy of apatite (3 0 0) adsorbed with $Al_2(SO_4)_3$ / $MgSO_4$ / Na_2SO_4 / K_2SO_4, $E(MSO_4)$ is the total energy of $Al_2(SO_4)_3$ / $MgSO_4$ / Na_2SO_4 / K_2SO_4, E(slab) is the total energy of apatite (3 0 0).

Results and discussion

Mechanism of phosphorite carbothermal reduction

Thermodynamic analysis

Phosphorite mainly consists of calcium fluoride phosphate, silicon dioxide, and silicon-calcium minerals, which may contain other metallic elements. The process of phosphorite reduction with carbon involves several steps: (1) Direct carbon thermal reduction of calcium fluoride phosphate, resulting in the production of yellow phosphorus. (2) Defluorination of calcium fluoride phosphate or its interaction with silicon dioxide to generate silicon fluoride and calcium phosphate. (3) The reduction of $Ca_5(PO_4)_3F$ by means of carbon leads to the generation of yellow phosphorus. (4) Formation of various calcium silicate compounds through the combination of silicon dioxide with the produced calcium oxide. The corresponding chemical reaction equations for these processes are provided below.

$$2Ca_5(PO_4)_3F + 15C = 9CaO + 15CO(g) + CaF_2 + 3P_2(g)\ R \quad (1)$$

$$Ca_5(PO_4)_3F = CaF_2 + 3Ca_3(PO_4)_2\ R \quad (2)$$

$$2Ca_5(PO_4)_3F + 9SiO_2 + 15C = CaF_2 + 15CO(g) + 9CaSiO_3 + 3P_2(g)\ R \quad (3)$$

$$Ca_3(PO_4)_2 + 5C = 3CaO + 5CO(g) + P_2(g)\ R \quad (4)$$

$$Ca_3(PO_4)_2 + 3SiO_2 + 5C = 3CaSiO_3 + 5CO(g) + P_2(g)\ R \quad (5)$$

$$nCaSiO_3 + mCaO = Ca_{n+m}Si_nO_{3n+m}\ R \quad (6)$$

The thermodynamic calculations of various reaction processes in the carbon-based reduction of phosphorite were carried out utilizing the HSC Chemistry software. The results, illustrating the Gibbs free energy (ΔG) for each reaction, are presented in Fig. 2. At standard atmospheric pressure, a negative value of Gibbs free energy implies that a reaction can proceed spontaneously in the forward direction. Therefore, by comparing ΔG changes with temperature for each reaction, we can determine whether a given reaction can occur under specific temperature conditions.

From Fig. 2**(a)**, The initial temperature of spontaneous carbothermal reduction reaction of $Ca_5(PO_4)_3F$ is 1534.73 °C, while the initial temperature is 1259.71 °C when SiO_2 is contained in the system. Similarly, the carbothermal reduction reactions of $Ca_3(PO_4)_2$ spontaneously take place at initial temperatures of 1476.57 °C and 1196.52 °C without and with SiO_2, respectively. This indicates that the presence of SiO_2 reduces ΔG of the reduction reactions, thereby lowering initial reaction temperatures and making $Ca_5(PO_4)_3F$ spontaneously undergo reduction reaction at a lower temperature.

The addition of sulfates facilitates the defluorination of $Ca_5(PO_4)_3F$ at lower temperatures, leading to the generation of calcium phosphate and the corresponding phosphate salts. The relevant chemical reaction equations are as follows.

$$2Ca_5(PO_4)_3F + 3Al_2(SO_4)_3 = 9CaSO_4 + CaF_2 + 6AlPO_4\ R \quad (7)$$

$$2Ca_5(PO_4)_3F + 9MgSO_4 = 9CaSO_4 + CaF_2 + 3\ Mg_3(PO_4)_2\ R \quad (8)$$

$$2Ca_5(PO_4)_3F + 9Na_2SO_4 = 9CaSO_4 + CaF_2 + 6Na_3PO_4\ R \quad (9)$$

$$2Ca_5(PO_4)_3F + 9K_2SO_4 + 6C + 9SiO_2 = 9CaSO_4 + CaF_2 + 3P_2O_3(g) + 6CO(g) + 9K_2SiO_3\ R \quad (10)$$

$$2AlPO_4 + 5C = Al_2O_3 + 5CO(g) + P_2(g)\ R \quad (11)$$

$$Mg_3(PO_4)_2 + 5C = 3MgO + 5CO(g) + P_2(g)\ R \quad (12)$$

$$2Na_3PO_4 + 5C + 3SiO_2 = 3Na_2SiO_3 + 5CO(g) + P_2(g)\ R \quad (13)$$

From Fig. 2**(b)**, it can be observed that the initiation temperature for the spontaneously carbothermal reduction reaction of calcium phosphate is 1477 °C, which is lower than the initial temperature of 1535 °C for the direct reaction between $Ca_5(PO_4)_3F$ and carbon. Additionally, the initiation spontaneous reaction temperatures for aluminum phosphate, magnesium phosphate, and sodium phosphate with carbon are significantly lower, at 1084 °C, 1227 °C, and 1122 °C, respectively.

Therefore, the addition of sulfates to the reaction system can lead to the formation of other phosphate salts that are more readily reduced, thereby reducing the initial temperature of spontaneous reaction, promoting the reduction, and augments the phosphorite conversion ratios.

Phase diagram of the reaction system with additives

In this study, the Factsage software was used to construct ternary phase diagrams for the $Ca_5(PO_4)_3F$-C-sulfate system under 101325 Pa and at a temperature of 1250 °C. The results are presented in Fig. 3.

Fig. 3 reveals that different proportions of reactants correspond to different product compositions, giving rise to multiple regions with distinct product compositions in the phase diagram. Find the position of first point located on the $Ca_5(PO_4)_3F$-C binary boundary, where the mass fraction of $Ca_5(PO_4)_3F$ and carbon is calculated for complete reaction. Then, using the red dashed line connect the first point and the second

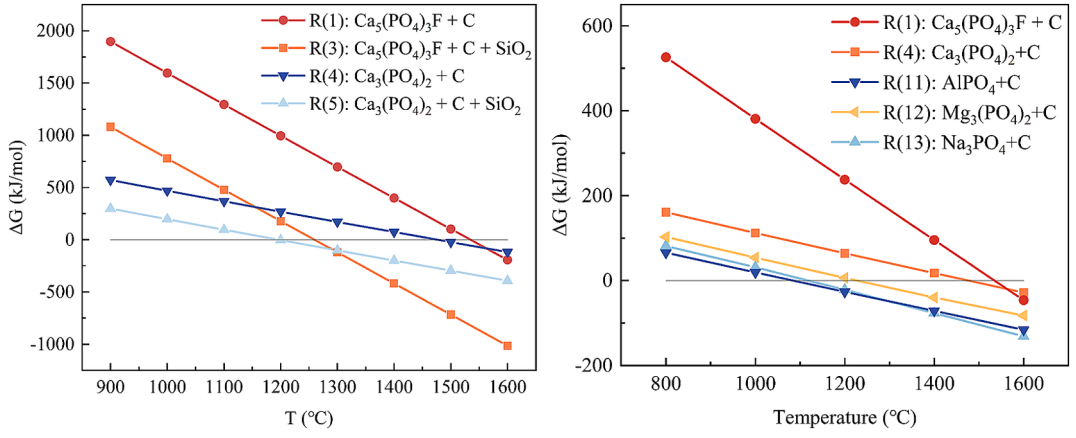

Fig. 2. Temperature-dependent Gibbs Free Energy variation for the carbothermal reaction of phosphorite (a) and the reaction with additives (b).

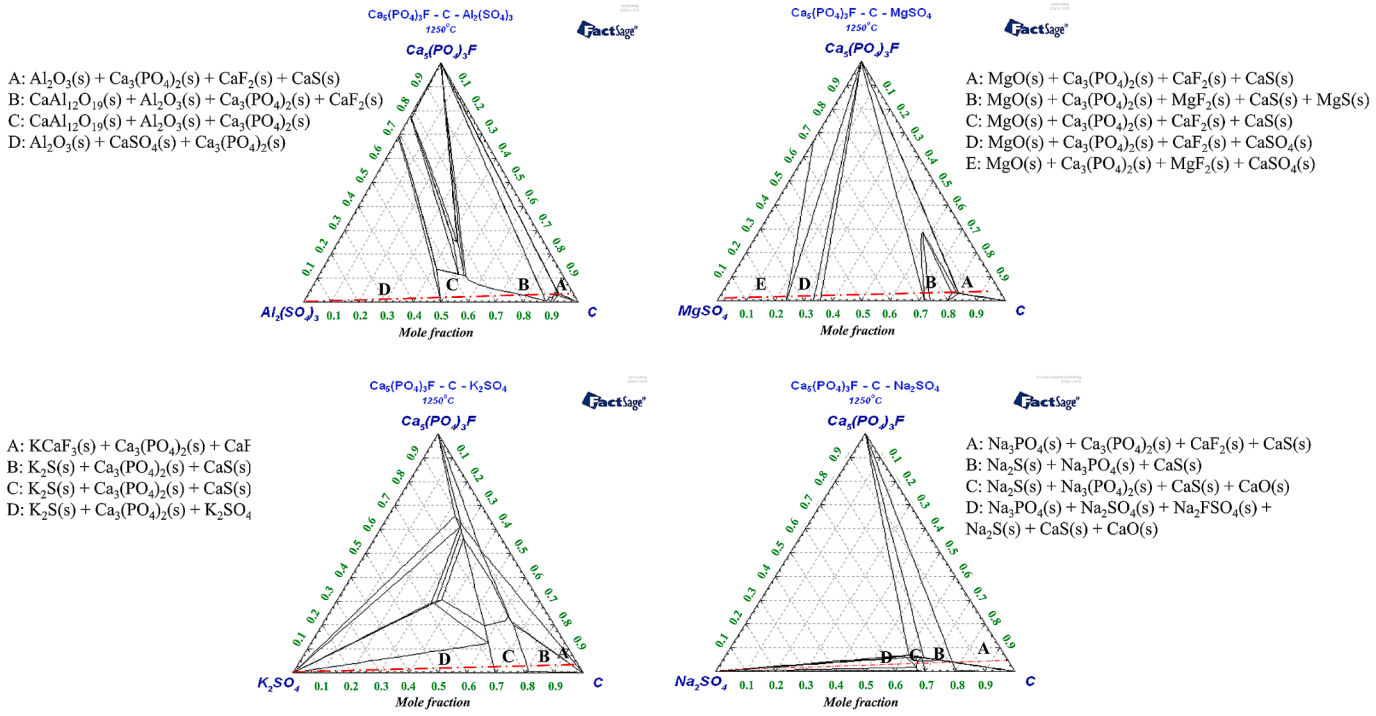

Fig. 3. Ternary phase diagram of $Ca_5(PO_4)_3F$-C-sulfate system at 1250 °C: (a) $Al_2(SO_4)_3$, (b) $MgSO_4$, (c) K_2SO_4, (d) Na_2SO_4.

point characterized by a zero mass fraction of sulfate, so we can establish a mixing line that exhibits a gradual increment in the sulfate addition ratio. It is evident from Fig. 3 that the adding sulfate leads to the appearance of calcium sulfide, calcium fluoride, calcium phosphate, the corresponding fluorides and phosphates in solid-phase products. As the sulfate addition ratio rises, a progressive transformation of calcium sulfide into calcium sulfate occurs, accompanied by the formation of corresponding metal oxides within the resultant products. This indicates that sulfate additives can promote the defluorination reaction of calcium fluoride phosphate, and they have the capacity to generate calcium phosphate or other phosphates that exhibit enhanced reactivity with carbon, consequently leading to an increase of phosphorite conversion ratio.

Thermogravimetric experiment

Fig. 4 **(a)** and **(b)** show the thermogravimetric and derivative thermogravimetric analysis results of six different samples, respectively: phosphorite, phosphorite with a silicon-to-calcium molar ratio of 2.0, and phosphorite with four different sulfates.

From Fig. 4**(a)**, a substantial weight loss in the phosphorite occurs at approximately 600 °C. This reduction in weight could be ascribed to the defluorination reaction of $Ca_5(PO_4)_3F$ at this particular temperature. Following the incorporation of silicon dioxide, the sample continues to display weight loss at approximately 600 °C, with a slight increment in the magnitude of this weight loss. This observation suggests that the added silicon dioxide reacts with the products of the defluorination reaction to form calcium silicate. Consequently, this promotes the forward reaction and increases the extent of defluorination. Upon the introduction of sulfate additives, the sample undergoes weight loss at even lower temperatures. This indicates that phosphorite engages in reactions with sulfate additives and silicon dioxide, leading to an increase of the silicon tetrafluoride gas production. Therefore, this process facilitates the transformation of calcium fluoride phosphate into calcium phosphate, calcium sulfate, and the associated phosphates at lower temperatures.

The peaks of the DTG curves of each group of samples in Fig. 4 **(b)** are analyzed to explore the effects of different additives on phosphorite in different temperature ranges. By analyzing the TG and DTG curves, the characteristic parameters of the weight loss of each group of samples at

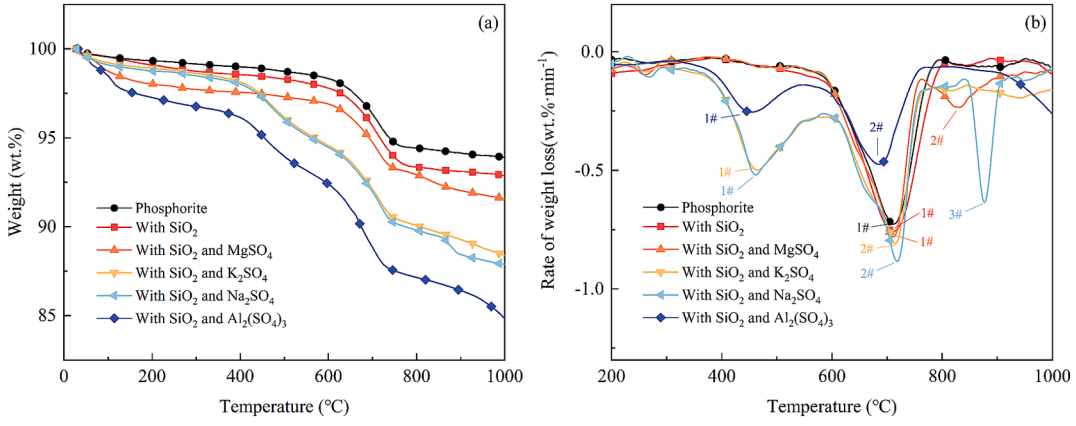

Fig. 4. Thermogravimetric experimental curves of phosphorite mixed with different additives in nitrogen atmosphere: (a) TG curves, (b) DTG curves.

different stages can be obtained, including weight loss, maximum rate of weight loss, temperature range of main reaction, and peak temperature. The numbers of each group of samples at each stage have been marked in Fig. 4 **(b)**, and the calculated results are summarized in Table 5. Table 5 reveals that adding silicon dioxide into the phosphorite brings about a marginal reduction in the initial temperature of the defluorination reaction. These cumulative alterations collectively streamline the reduction reaction of the phosphorite, rendering it more facile. The introduction of sulfate additives to the phosphorite gives rise to weight loss within the temperature interval of 400–500 °C. It suggests that calcium fluoride phosphate engages in reactions with the additives within this specific temperature range. This directly accelerates the defluorination of calcium fluoride phosphate, decreases the temperature of initial reaction, extends the temperature range of reaction, and enhances the weight loss rate, thus improving its conversion ratio.

Optimal conditions in a bubbling fluidized bed

To investigate the optimal process parameters of the carbothermal reaction of phosphorite in the bubbling fluidized bed reactor, a sequence of experiments was carried out at 1250 °C. These experiments involved variations in reaction time, U_{op} of the carrier gas, carbon excess ratio, and silicon-calcium molar ratio. Different conditions were tested to determine their effects on the phosphorite conversion. Three different types of phosphorites were used for comparative experiments to explore the universality of the experimental results. In this study, three groups of experiments were performed for each operational condition, and the experimental outcomes were averaged. Fig. 5 illustrates the relationships between the phosphorite conversion ratio and key influencing factors.

From Fig. 5**(a)**, this phenomenon is evident that the reaction time exerts the most pronounced influence on the conversion ratios of phosphorite during carbothermal reduction. An extension in reaction time leads to a corresponding increase in the phosphorite conversion ratios. This is obvious that the reactions are intense during the first 40 min, and the differences in conversion ratios among these three types of phosphorite are minimal. After 40 min, the phosphorite with the highest grade shows the best reducibility.

In this study, the conversion ratios of three types of low- and medium-grade phosphorite reached 78.55 %, 77.29 %, and 76.50 %, respectively, under fluidized bed conditions at 1250 °C for 80 min. By comparison, previous studies [34,35] indicate that the phosphorite reduction in a kiln at 1250 °C typically achieves conversion ratios ranging from 60 % to 70 %, while fixed-bed systems under similar conditions generally exceed 65 % [36,37,38]. The results of this research emphasize the advantages of the dynamic fluidization state in a fluidized bed, as it promotes material contact and ensures uniform temperature distribution inside the reactor. Furthermore, the simple structure and high throughput capacity of a bubbling fluidized bed facilitate the continuous phosphorite reduction, improving production efficiency and profitability.

As illustrated in Table 6, it can be observed that the growth value of phosphorite conversion ratio declines within the same reaction time interval. This suggests that although phosphorite conversion ratio is increasing, the growth rate of its conversion ratio decelerates with the prolongation of the reaction time.

When the reaction time was extended from 5 min to 20 min, the conversion ratios of these three phosphorites exhibited a 23.82 %, 23.87 %, and 25.08 % increase, respectively. At the commencement stage of phosphorite reduction, the interaction between the reactants, including phosphorite and the reducing agent, is just beginning. During this phase, the reaction system exhibits high activity, characterized by an abundance of active sites on the phosphorite surface. These active sites facilitate effective contact with the coal, thereby enabling rapid progression of the reaction. Upon extending the reaction time from 20 min to 40 min, the conversion ratios of the three phosphorites exhibited a notable increase, reaching 18.40 %, 17.67 %, and 18.97 %, respectively. As the reaction proceeds, the reactants are continuously consumed, and the active loci on the phosphorite surface are gradually occupied or covered by the products. This coverage diminishes the effective contact area among phosphorite and coal, leading to a decline in the reaction rate. Upon extending the reaction time from 40 min to 60 min, the conversion ratios of the three phosphorites exhibited an increase of 9.377 %, 8.263 %, and 9.167 %, respectively. Upon extending the reaction time from 60 min to 80 min, the conversion ratios of the three phosphorites exhibited an increase of 7.331 %, 8.370 %, and 7.619 %, respectively. At this stage, the reactant concentrations have significantly decreased, bringing the reaction closer to equilibrium. The residual unreacted phosphorite may exhibit low reactivity due to its structural properties, limiting further reaction progress. Additionally, the accumulation of intermediates can promote side reactions, further impeding the main reaction and resulting in a slower reaction rate.

After 80 min, the distinctions in conversion ratios among the three varieties of phosphorites gradually diminish, and further extending the reaction time does not significantly increase the conversion ratio. For energy-saving purposes, the maximum reaction time chosen in the experiment is 80 min.

From Fig. 5 **(b)**, An escalation in the carbon excess ratio enhances the contact area among phosphorite particle and coal particle, promoting the progression of the forward reaction, then accelerating the reaction rate. However, the ash content in coal contains a variety of inorganic minerals that can interact in complex ways with the components of phosphorite under high temperature. Specifically, metal oxides such as iron and calcium present in the coal ash can react with phosphorus to form compounds such as iron phosphide and calcium ferrophosphate. These compounds are challenging to reduce, thereby impeding phosphorus release and reducing the overall conversion ratio of phosphorite. Additionally, interactions between metal oxides in the coal ash and silicon dioxide can decrease the silicon content, further hindering the defluorination reaction of calcium fluorophosphate and ultimately lowering the conversion ratio of phosphorite. Therefore, selecting an appropriate carbon excess ratio is crucial for optimizing the conversion

Table 5
The parameters of weightlessness characteristics for each sample.

Sample	Number	Weight Loss (wt.%)	Maximum rate of weight loss (wt.%·min^{-1})	Temperature range of main reaction (°C)	Peak temperature (°C)
Phosphorite	1#	3.76	−0.7274	613.86–788.54	711.94
With SiO_2	1#	4.35	−0.7930	612.90–808.86	711.05
With $MgSO_4$	1#	1.55	−0.0783	78.90–374.86	252.44
	2#	4.83	−0.7343	556.88–862.52	703.78
With Na_2SO_4	1#	10.22	−0.5185	357.96–962.26	460.79
	2#	6.32	−0.8834	589.15–920.26	717.34
	3#	2.25	−0.6346	757.46–998.93	876.96
With K_2SO_4	1#	9.79	−0.4988	353.75–971.50	464.53
	2#	6.75	−0.8081	556.29–989.57	715.33
With $Al_2(SO_4)_3$	1#	10.95	−0.2541	231.57–928.67	452.85
	2#	7.57	−0.4742	471.27–820.88	684.70

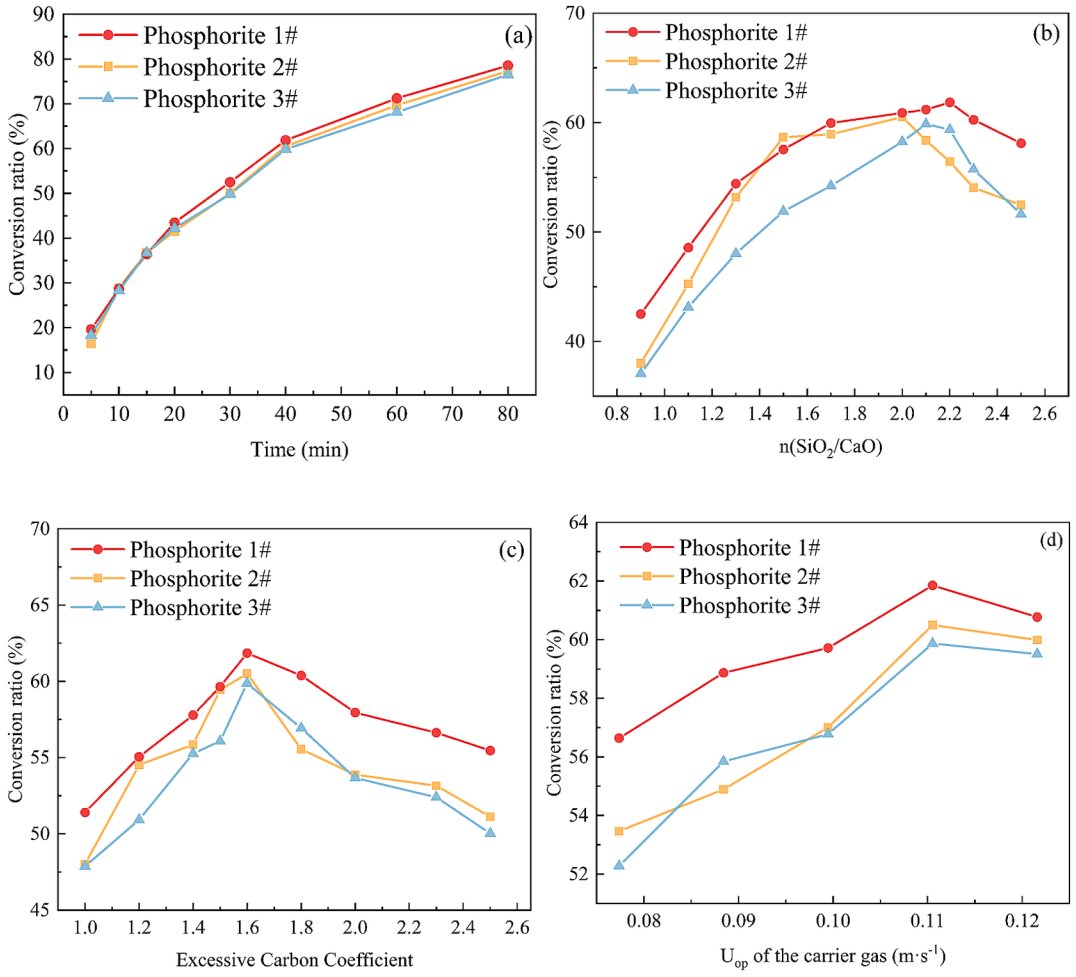

Fig. 5. The relationship between the conversion ratio of phosphorite and reaction time (a), silicon-calcium molar ratio (b), excess carbon coefficient (c), and U_{op} of the carrier gas (d).

Table 6
Incremental in conversion ratio for different reaction time intervals.

Interval of reaction time (min)	1# Phosphorite	2# Phosphorite	3# Phosphorite
5–20	23.82 %	23.87 %	25.08 %
20–40	18.40 %	17.67 %	18.97 %
40–60	9.377 %	8.263 %	9.167 %
60–80	7.331 %	8.370 %	7.619 %

ratio of phosphorite. The optimal carbon excess ratio of these three types of phosphorite are all around 1.6.

As is observable from Fig. 5 **(c)**, adjusting silicon-calcium molar ratio of the sample to about 2.0–2.2 is beneficial to improving the conversion ratio of phosphorite. The appropriate silicon-calcium molar ratio can promote the defluorination of calcium fluorophosphate to form calcium phosphate, thereby promoting the direct reduction reaction with carbon and reducing the temperature of initial spontaneous reaction. The fluxing effect of silicon dioxide increases the contact area between materials, making it easier for the phosphorite to react with coal particle. Nevertheless, excessive silicon dioxide can reduce the grade of phosphorite, absorb more heat, and lead to the excessive formation of calcium silicates, which can hinder contact between coal particle and phosphorite. These factors ultimately diminishing the conversion ratio of the reaction.

It can also be found from Fig. 5 **(c)** that the optimal value of the silicon-calcium molar ratio varies depending on the type of phosphorite. Through comparative analysis, it was found that this may be related to the original silicon dioxide content of the phosphorite. The SiO_2 content in 1# phosphorite is the lowest (21.52 %), so the phosphorite conversion ratio can reach the maximum value when its silicon-calcium molar ratio is large (2.2). The SiO_2 content in 2# phosphorite is the highest (37.52 %), so the phosphorite conversion ratio can reach the maximum value when its silicon-calcium molar ratio is small (2.0). Previous studies [39–41] also have shown that SiO_2 has the effect of promoting defluorination reaction and reducing reaction temperature in phosphorite reduction reaction, which is beneficial to improving the phosphorite conversion ratio. When the SiO_2 content in the phosphorite itself is large, there is sufficient SiO_2 in the system to participate in the reaction. If the silicon-calcium molar ratio is too large, SiO_2 will hinder the contact probability between calcium fluorophosphate and the reducing agent, and will also generate too much calcium silicate, which will wrap the unreacted phosphorite particles and is not conducive to the reaction. Excessive SiO_2 will also absorb reaction heat, further hindering the reduction reaction. If the SiO_2 content in the phosphorite is low, there is insufficient SiO_2 in the system to participate in the reaction. The amount of SiO_2 cannot fully meet the requirements of promoting defluorination reaction and reducing reaction temperature. As the silicon-calcium molar ratio increases, more SiO_2 participates in the reaction, which can fully play its role in promoting the reaction and improve the phosphorite conversion ratio. Therefore, when the original SiO_2 content in the phosphorite is relatively low, the phosphorite conversion ratio can reach its maximum value when the silicon-calcium molar ratio is large.

In a fluidized bed reaction, the U_{op} of the carrier gas affects the

fluidization condition and particle collision intensity in the bubbling fluidized bed. Fig. 5 **(d)** shows that with the increase of the U_{op}, the phosphorite conversion ratio shows a trend of first increasing and then decreasing. The U_{op} of the carrier gas for the three phosphorites is 0.11 m•s^{-1}. This is because when the U_{op} is too low, the particles cannot be fully fluidized, resulting in uneven distribution of particles in the bed, and some particles will even accumulate on the distribution plate, which greatly limits the contact between the particles and the reactants, thereby affecting the reaction and making the phosphorite conversion ratio low. As the U_{op} of the carrier gas gradually increases, the bed fluidization effect is improved, the particles can fully move in the bed, the contact with the reducing agent coal particles is more sufficient, and the heat transfer is more uniform, which is conducive to the phosphorite reduction reaction, so the phosphorite conversion ratio gradually increases. However, when the U_{op} is too high, the gas will stay in the bed for too short a time, and some reactants will be carried out of the reaction zone before they can fully react, and gather in the lower temperature area at the top of the reactor. This is not conducive to the continued reaction and ultimately leads to a decrease in the phosphorite conversion ratio.

From Fig. 5, it is evident that phosphorite with a higher grade typically has a higher conversion ratio. The content of calcium fluorophosphate in high-grade phosphorite is relatively high, whereas low-grade phosphorite typically contains more impurities. During the reduction reaction, calcium fluorophosphate serves as the primary reactant, and its content directly influences the progression of reaction. The elevated impurity levels in low-grade phosphorite occupy physical space, reducing the effective contact area between the active reactants, such as calcium fluorophosphate and coal. Furthermore, these impurities may engage in side reactions with either the reactants or the intermediates, altering the reaction environment, including parameters like pH, which can affect equilibrium and kinetics of the reaction. Additionally, the crystal structure of high-grade phosphorite is typically more orderly, facilitating the reaction process. In contrast, low-grade phosphorite often exhibits structural defects or distortions due to the presence of impurities. Such irregularities in the crystal lattice can impede the diffusion of reactants and intermediates and disrupt energy transfer. These factors collectively slow down the rate of reaction and lower the overall low-grade phosphorite conversion ratio.

In summary, a reaction time of 60 min, a silicon-calcium molar ratio falling within the range of 2.0–2.2, a carbon excess ratio of 1.6, and a gas flow rate set at 500 L/h are chosen for industrial applications and subsequent experiments, which can achieve cost reduction and ensure a high conversion ratio.

Influence of additives on phosphorite conversion ratio

Due to the temperature limitations of the fluidized bed reactor, calcium fluoride phosphate cannot directly undergo a reduction reaction with carbon or rapidly undergo defluorination at 1250 °C. However, the addition of sulfates can promote the defluorination of calcium fluoride phosphate, and generate phosphate salts and calcium phosphate. These compounds are inherently more amenable to reduction by carbon, thereby increasing the reaction rate and phosphorite conversion ratio. Therefore, with the aim of promoting the reduction reaction and improve the conversion ratio of phosphorite, 2# phosphorite was selected for this experiment. The raw materials were mixed at a silicon-calcium molar ratio of 2 and a carbon excess ratio of 1.6, with the addition of sulfates, aluminum sulfate, magnesium sulfate, sodium sulfate, and potassium sulfate. According to the research of Qian Yang [9], subjecting phosphorite to a pretreatment process within the temperature range of 600–900 °C for a duration of 20 min facilitates phosphorite conversion ratio. Given the susceptibility of sulfate to thermal decomposition at elevated temperatures, a selection of 700 °C was made for the pretreatment temperature to safeguard sulfate decomposition, thereby ensuring an optimal improvement in phosphorite conversion ratio. Consequently, the specimens underwent a pretreatment regimen in a muffle furnace set at 700 °C for a duration of 20 min and cooled before being placed in a fluidized bed. The reduction reaction took place at 1250 °C and 0.11 m•s^{-1} of the carrier gas for 60 min. The resulting products were analyzed to investigate the impact of sulfate additives and determine the optimal additive ratio (using the molar mass of pentoxide phosphorus in phosphorite as the basis). The results are shown in Fig. 6.

From Fig. 6, it is obvious that adding sulfates into phosphorite leads to an improvement in the conversion ratio, regardless of whether pretreatment of the phosphorite is performed. The phosphorite conversion ratio initially increases and then decreases with the increase in the proportion **o**f the four sulfate additives. This indicates that the introduction of an appropriate amount of sulfate can promote the carbothermal reduction reaction. However, excessive additives can reduce the grade of phosphorite. Moreover, excess sulfates can generate corresponding oxides and silicates, which can combine with the calcium oxide in the reaction product to form alumina, magnesia, potash, and soda-containing crystalline phases. These products tend to adhere to the unreacted phosphorite surface, obstructing contact with the reducing agent and reducing the contact area of the reactants, which leads to a weakening of the conversion ratio. As shown in Fig. 6, without pretreatment, the optimal additive ratios for aluminum sulfate, magnesium sulfate, potassium sulfate, and sodium sulfate are 12 %, 10 %, 3.5 %, and 4.5 %, respectively. Among them, potassium sulfate has the most significant promoting effect of phosphorite reduction, which increases the phosphorite conversion ratio from 58.43 % without additives to 72.96 %. Compared to the untreated reaction system, the conversion ratio is higher after pre-treatment. The optimal additive ratios for aluminum sulfate, magnesium sulfate, potassium sulfate, and sodium sulfate are 12 %, 8 %, 3.5 %, and 5 %, respectively. Among them, aluminum sulfate has the most significant promoting effect of carbothermal reduction, increasing the phosphorite conversion ratio from 63.57 % without additives to 79.95 %.

After collecting the residue under different reaction temperature conditions and with various sulfates at 1250℃ form a bubbling fluidized bed, the products were analyzed by a X-ray diffractometer. Fig. 7 presents the analysis outcomes of the corresponding products.

As is observable from Fig. 7, the main components in the products of the phosphorite carbothermal reduction are $Ca_5(PO_4)_3F$, SiO_2, and various forms of calcium silicate. With the elevation of the temperature of phosphorite reduction, calcium phosphate peaks and silicon dioxide peaks in the products gradually decrease, peaks indicative of calcium phosphate and calcium silicate emerge and become more pronounced. The characteristic peaks of calcium fluorophosphate and silicon dioxide in the product composition after adding sulfates were weakened, while the characteristic peaks of calcium silicate were enhanced. This indicates that sulfates can promote the defluorination of calcium fluoride phosphate, thereby giving rise to the generation of a greater amount of calcium oxide. Therefore, sulfate additives do not affect the overall reaction progress of the carbothermal reduction but rather act as intermediate reactants to promote the defluorination of calcium fluoride phosphate, reduce the reaction activation energy, and enhance phosphorite conversion ratio.

Additionally, nine representative mineral slag samples based on the optimal conditions for phosphorite reduction within a fluidized bed reactor and the optimal additive ratios for the four additives were selected. These samples were analyzed for their microstructural morphology and composition. The obtained results are shown in Fig. 8.

As is observable from Fig. 8, the microscopic morphology of slag under different reaction temperatures and additive conditions is different. At 1100 °C and 1150 °C, the reduction products exhibit a uniform distribution, rough surface texture, and dense block-like structures with numerous small particles. This particular microstructure impedes both heat and mass transfer, leading to incomplete phosphorite reduction and subsequently lower conversion ratio. At a reaction temperature of 1200 °C, the product surface exhibits signs of particle

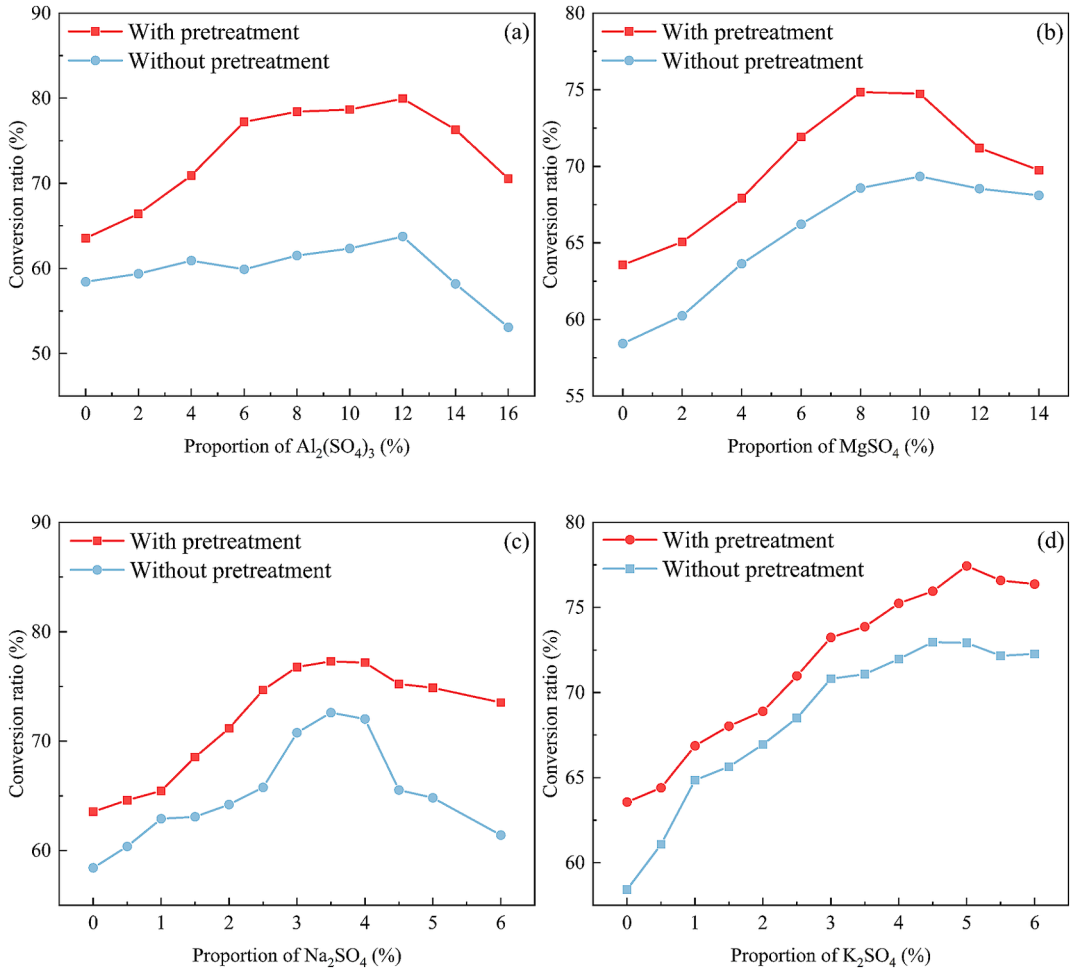

Fig. 6. The influence of adding (a) $Al_2(SO_4)_3$, (b) $MgSO_4$, (c) Na_2SO_4, and (d) K_2SO_4 with different proportion on the conversion ratio of phosphorite.

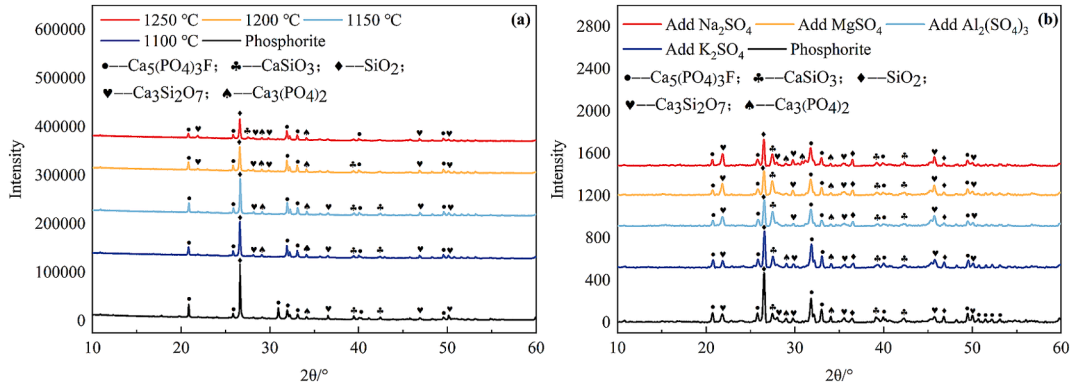

Fig. 7. XRD of product, (a) product of different reaction temperature, (b) product of adding different sulfates.

agglomeration and sheet-like fractures, thereby enhancing the contact between phosphorite and reactants, which leads to improved heat absorption. the surfaces of the products become smoother with fewer small particles. Instead, more and larger pores appear in the microstructure. This facilitates improved heat transfer and increases the contact area for reactions, ultimately enhancing phosphorite conversion ratio.

Adding sulfates leads to smoother product surfaces with distinct layered structures, increased numbers and sizes of pores, and a more porous slag texture. This enhances the efficiency of heat and mass transfer processes, facilitating a more effective utilization of heat and reducing agents during the reduction reaction, consequently increasing the yield of yellow phosphorus.

The EDS results obtained from the surface scans of the phosphorite reduction slag are shown in Fig. 8 and summarized in Table 7. When reaction temperature rises to above 1250 °C, the content of Ca decreases significantly, indicating that high temperature is conducive to the participation of Ca in various reactions to form complex compounds, thereby changing its distribution state and content ratio in the product. As the reaction temperature increases, the content of P element generally shows a downward trend, indicating that more calcium fluorophosphate is reduced by carbon and the generated yellow phosphorus leaves the reaction system. The content of Si element increases

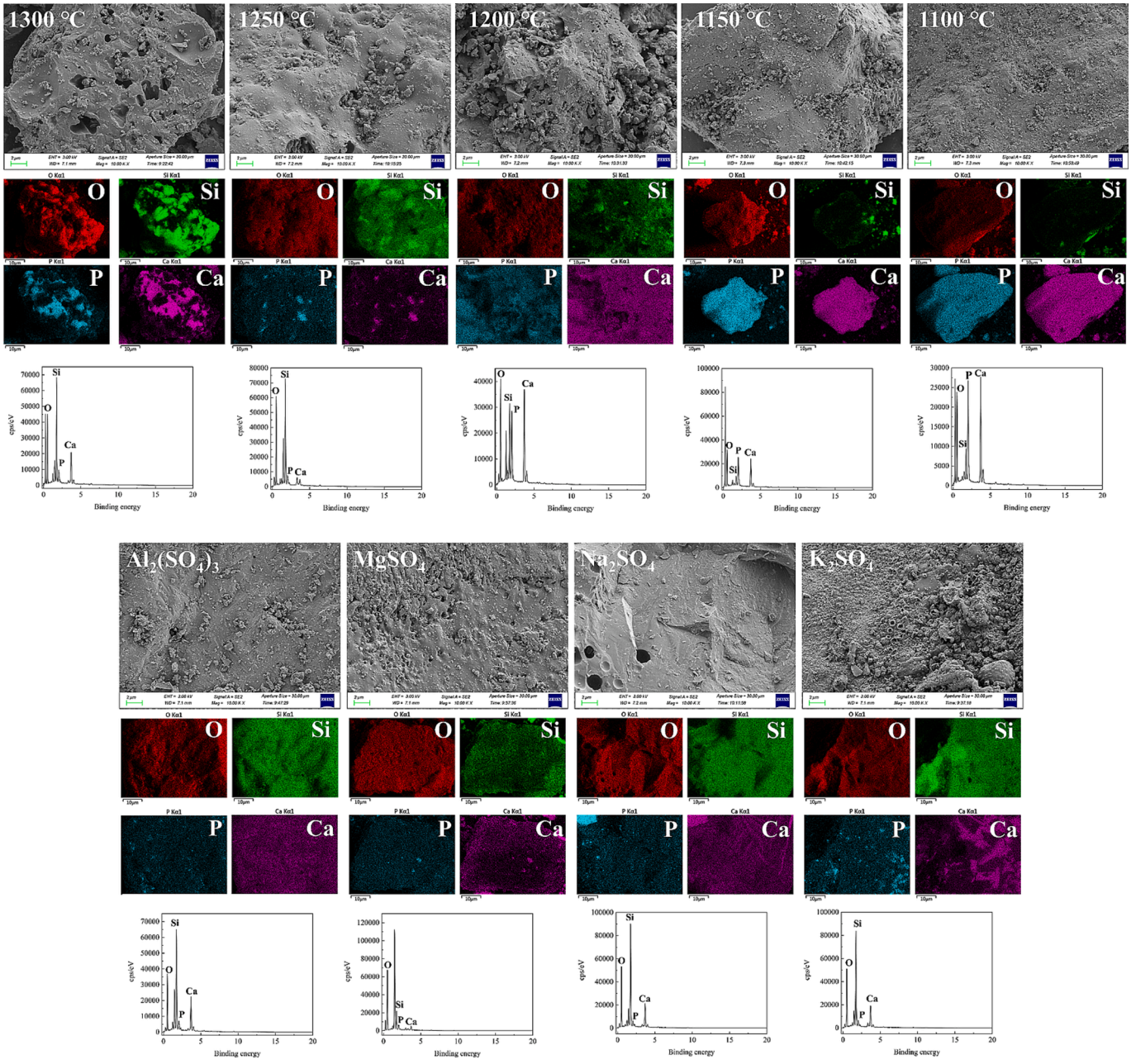

Fig. 8. SEM-EDS spectrum of phosphorite reduction residue.

Table 7
Analysis of average mass percentage of EDS elements in phosphorite reduction products (%).

Sample	Ca	P	Si	O
1100 °C –None	33.71	15.16	4.08	47.04
1150 °C – None	28.92	13.42	3.93	53.72
1200 °C – None	30.20	10.75	10.15	48.90
1250 °C – None	4.77	2.29	35.66	57.27
1300 °C – None	19.36	2.78	26.40	51.46
1300 °C – $MgSO_4$	7.44	1.97	16.54	74.05
1300 °C –K_2SO_4	16.94	1.24	30.70	51.12
1300 °C –Na_2SO_4	17.61	0.96	30.82	50.61
1300 °C – $Al_2(SO_4)_3$	23.03	1.34	27.53	48.10

significantly after the temperature exceeds 1200 °C. This shows that at higher temperatures, silicon dioxide reacts more with calcium fluorophosphate and other components to generate silicon-containing compounds. This reaction further promotes the reduction process, thereby elevating phosphorite conversion ratio. This indicates that more calcium fluoride phosphate is being carbon-reduced to produce CaO and yellow phosphorus, which exit the reaction system. Conversely, the content of Si (silicon) element continues to increase with the rising temperature. This phenomenon indicates that higher temperatures encourage the participation of SiO_2 in the defluorination reaction of calcium fluoride phosphate. Simultaneously, SiO_2 reacts with the reduction product CaO to create $CaSiO_3$. This reaction further promotes the advancement of the reduction process and leads to an increased conversion ratio of phosphorite.

Furthermore, the inclusion of sulfates leads to a noticeable decrease in the phosphorus content, whereas the silicon content keeps growing. This occurrence implies that the elevation of temperature makes silica more involved in the defluorination reaction of calcium fluorophosphate, and at the same time combined with the reduction products of calcium oxide to generate calcium silicate, thereby advancing the

reduction and enhancing phosphorite conversion ratio. These results are consistent with the conclusions derived from the mechanistic analysis and experimental findings discussed previously.

This study explored the adsorption characteristics of four different sulfates and apatite through molecular dynamics simulation to explore the intrinsic reasons for their influence on phosphorite reduction. The results are shown in Fig. 9. The E_{ad} of the four sulfates and apatite are all negative, which means that the adsorption process is an exothermic process, which is thermodynamically spontaneous. The larger the absolute value of E_{ad}, the more energy is released in the adsorption process, the more stable the adsorption configuration is, and the easier it is for the adsorbate to bind to the surface. The E_{ad} of $Al_2(SO_4)_3$ is −7.49 eV, and its absolute value is the highest among the four sulfates. The E_{ad} of K_2SO_4 is −6.61 eV, and its absolute value is relatively high. The E_{ad} of Na_2SO_4 and $MgSO_4$ are −5.11 eV and −5.85 eV, respectively, and their absolute values are relatively small. This shows that $Al_2(SO_4)_3$ releases the most energy during the adsorption process and forms the most stable adsorption configuration. Therefore, among the four sulfates, $Al_2(SO_4)_3$ is more likely to bind to the apatite surface, promoting its reaction to generate phosphates that are more easily reduced. Moreover, this strong adsorption is also very likely to significantly change the electron cloud distribution and chemically active sites on the apatite surface, creating more favorable conditions for the phosphorite reduction reaction, thereby increasing the conversion ratio of the phosphorite. In previous experimental results, the conversion ratio of carbon thermal reduction of phosphorite after pretreatment with $Al_2(SO_4)_3$ was the highest, followed by K_2SO_4. Na_2SO_4 and $MgSO_4$ were relatively low. This phenomenon is consistent with the calculation results of molecular dynamics simulation, further verifying the promoting effect of the four sulfates on the reduction of phosphorite.

Kinetic analysis

Phosphorite conversion ratio under various reduction time

A sample of 2# phosphorite was chosen, and the conditions were set to a silicon-calcium molar ratio of 2.0, a carbon excess ratio of 1.6, and 0.11 m•s^{-1} of the carrier gas. The four sulfates, each added in optimal proportions, were incorporated into the raw materials, which were subsequently subjected to a pre-treatment process. The connection among the conversion ratio of each sample and reaction time was investigated under three temperature conditions: 1150 °C, 1200 °C, and 1250 °C. The results are shown in Fig. 10.

Fig. 10 demonstrates the increasing trend of the phosphorite conversion ratio as the reaction time prolongs. The conversion ratio of both additive-free and additive-assisted systems exhibits a rapid increase during the first stage (0–40 min) of the phosphorite reduction. This can be attributed to the high effective collision frequency of reactant molecules at the early stage, which accelerates the reaction rate and facilitates a swift rise in the conversion ratio. During the later stage of the reaction (40–80 min), the reaction approaches equilibrium, leading to a reduction in the amount of convertible phosphorite and a gradual decline in the reaction rate.

Under identical conditions, higher reaction temperatures significantly augment phosphorite conversion ratio. Elevated temperatures provide the requisite energy to accelerate the reaction, consistent with the endothermic nature of phosphorite reduction. Without sulfate additives, the phosphorite conversion ratio is the lowest under the same conditions. At 1150 °C, the differences in conversion ratios between additive-assisted systems and the additive-free system are relatively minor. However, at 1250 °C, the discrepancies become pronounced, suggesting that higher temperatures facilitate additive participation, modify the activation energy, and influence the reaction pathway, thereby promoting the reduction reaction.

When reacted at 1250 °C for 60 min, the phosphorite conversion ratio without sulfate additives was limited to 69.67 %. Different

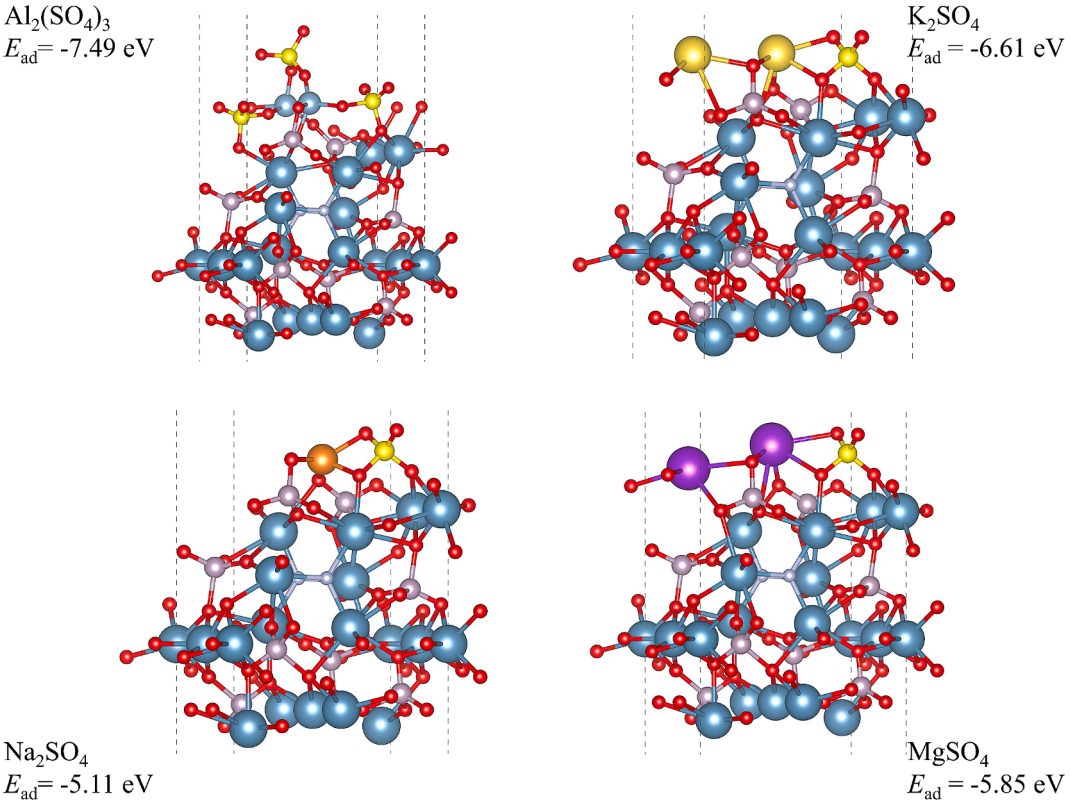

Fig. 9. Calculation results of adsorption energy of four sulfates on apatite.

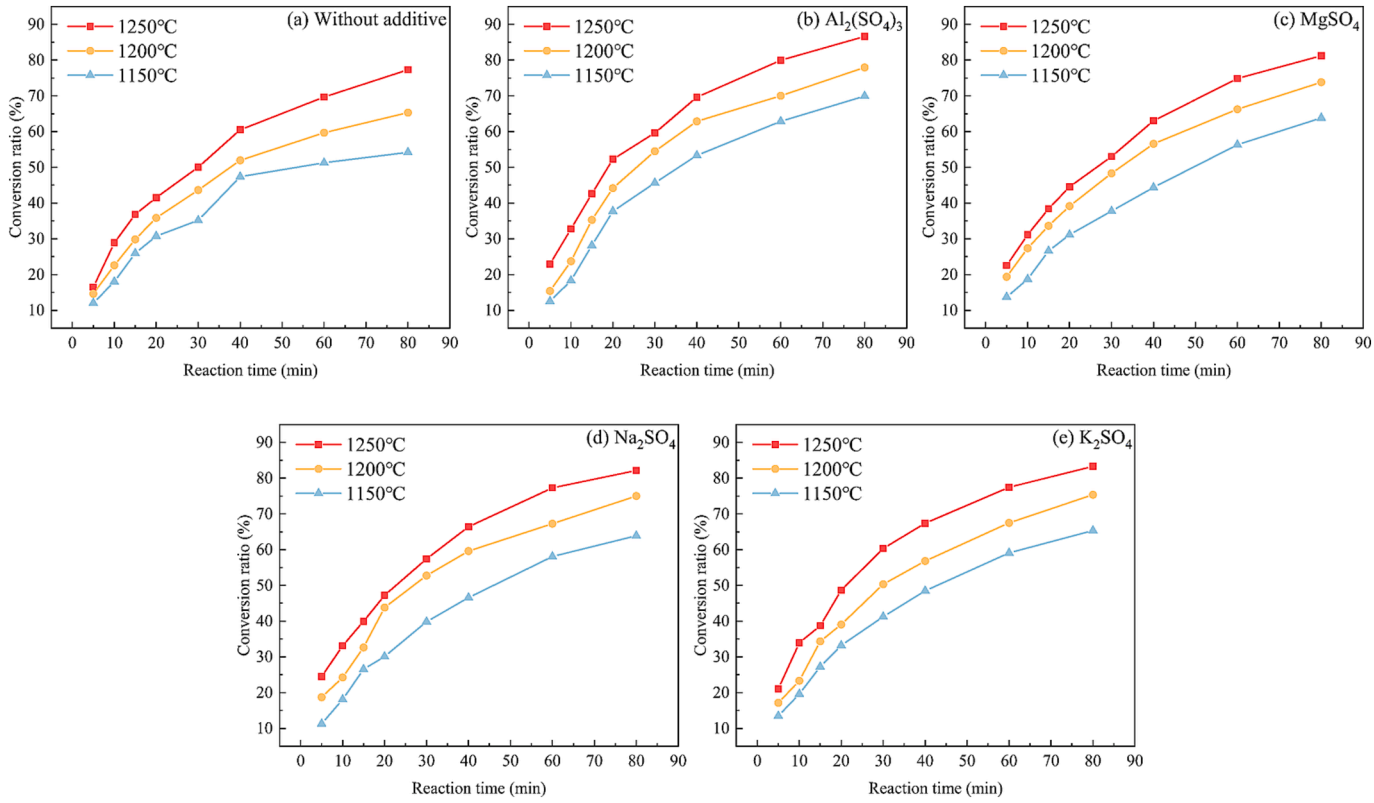

Fig. 10. The relationship between the conversion ratio of phosphorite and reaction time: (a) Without additive, (b) $Al_2(SO_4)_3$, (c) $MgSO_4$, (d) Na_2SO_4, (e) K_2SO_4.

additives exhibited varying degrees of influence on the reaction, resulting in noticeable differences in their efficacy in promoting phosphorite reduction. Among the tested additives, $Al_2(SO_4)_3$ demonstrated the most significant enhancement, achieving a conversion ratio of 79.95 %. In comparison, $MgSO_4$ displayed a weaker promotion effect, with a conversion ratio of 74.85 %.

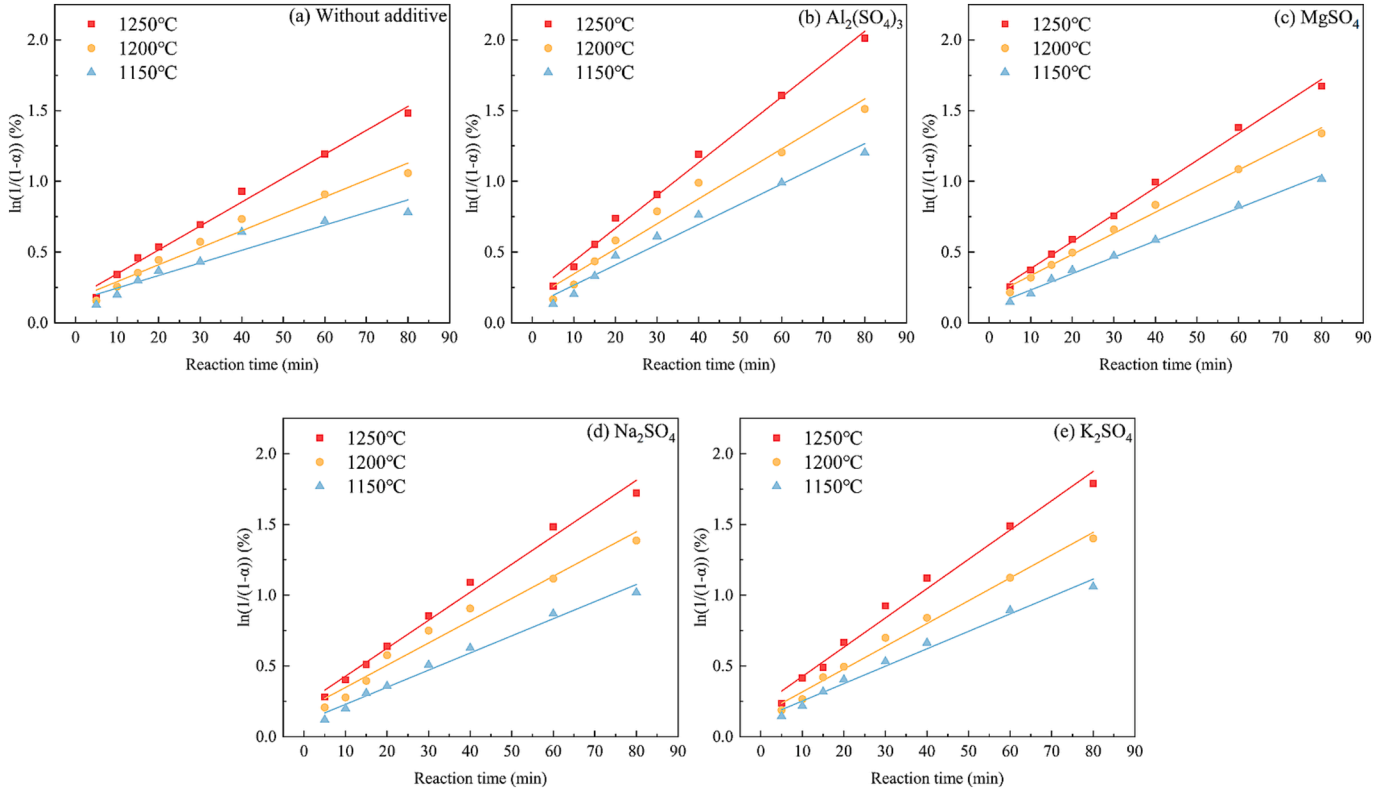

Fig. 11. Relationship between ln[1/(1-α)] and reaction time in phosphorite: (a) without addition, (b) $Al_2(SO_4)_3$, (c) $MgSO_4$, (d) Na_2SO_4, (e) K_2SO_4.

Determination of reaction order

According to previous studies, scholars [42,43] generally believe that the carbon thermal reduction reaction process of phosphorite can be described by a first-order reaction model. Therefore, this experiment explored the relationship between the logarithm of the conversion ratio $\ln(1/(1-\alpha))$ and the reaction time under different working conditions. The $\ln(1/(1-\alpha))$ of the carbothermal reduction conversion of phosphorite in different reaction systems at 1150 ℃, 1200 ℃ and 1250 ℃ was plotted against the reaction time (α is the phosphorite conversion ratio). As shown in Fig. 11, the regression curves were obtained by curve-fitting the scattering points of the same condition in the graph, respectively.

The inclinations of the curves within the graph signify the reaction rate constants (k) corresponding to each temperature. The coefficient of determination (r^2) was computed via linear regression. Table 8 compiles the curve fitting outcomes. In light of the data in Table 8, the values of r^2 values at each temperature are close to 1, indicating that the first-order reaction model can accurately capture the trend of the conversion ratio with respect to time during the reaction process. This phenomenon shows that the model has high reliability and effectiveness in describing the kinetics of phosphorite carbothermal reduction reaction.

From Table 8, it can be seen that $k_{(\text{Without additive})}$ is always less than $k_{(\text{Adding sulfate})}$ at the same temperature, which can prove that the addition of sulfate additive can promote the phosphorite carbothermal reduction reaction. The r^2 values under different systems increase gradually with increasing temperature and are close to 1. This indicates that the addition of sulfates does not change the carbon thermal reduction mechanism of phosphorite, which still conforms to a first-order reaction. Moreover, as the temperature increases, this trend becomes more pronounced, further confirming that sulfate additives act as catalysts in the reaction.

Apparent activation energy calculation

Referring to the methods in previous studies [10,34], the data of phosphorite conversion ratio at different reaction temperatures and reaction times can be uesd to perform kinetic analysis and calculate the corresponding activation energy. This study summarizes the conversion ratio of phosphorite reduction in a fluidized bed. Based on the obtained data, ln k versus $1/T$ relationship curves were plotted, as shown in Fig. 12. Curve fitting procedures were employed to analyze the obtained results, with details outlined in Table 9. In accordance with the Arrhenius equation, the inclination of the fitted curve represents $-E/R$, from which the activation energy for each reaction in both systems can be determined [44,45].

$$k = A\exp\left(-\frac{E}{RT}\right) \tag{2}$$

$$\ln k = \ln A - \frac{E}{RT} \tag{3}$$

In these equations, A represents the pre-exponential factor (min^{-1}), E is the activation energy (kJ·mol^{-1}), R is the molar gas constant ($\text{kJ·mol}^{-1}\text{·K}^{-1}$), and T is the temperature (K).

As is observable from Table 9, the correlation coefficients for the fitted curves of five samples approach 1, indicating that the results of experiments and the choice of reaction order in the experiments is reasonably justified. It is evident that $E_{(\text{Without additive})} > E_{(\text{Potassium sulfate})} > E_{(\text{Magnesium sulfate})} > E_{(\text{Sodium sulfate})} > E_{(\text{Aluminum sulfate})}$. Without the addition of sulfate, the activation energy for the carbothermal reduction of phosphorite is 115.25 kJ·mol^{-1}. With the addition of aluminum sulfate, magnesium sulfate, sodium sulfate, and potassium sulfate, the activation energy of the reaction decreases by 28.11 kJ·mol^{-1}, 24.78 kJ·mol^{-1}, 26.67 kJ·mol^{-1}, and 21.52 kJ·mol^{-1}, respectively. It is worth highlighting that aluminum sulfate demonstrates the most pronounced effect in reducing the reaction activation energy, consistent with the experimental findings that aluminum sulfate exerts the most substantial influence on phosphorite conversion ratio following pretreatment. Consequently, in light of the activation energy analysis, the incorporation of additives in carbothermal reactions is capable of considerably diminishing the activation energy, augmenting the reaction rate, and facilitating the reaction. This accomplishes the goals of energy efficiency and cost reduction. Fig. 13 shows the mechanism of phosphorite with sulfate additives reduction in a fluidized bed.

Table 8
Reaction rate constants (k) and correlation coefficients (r^2) under varying temperatures.

Additive		1150 °C	1200 °C	1250 °C
None	k/min^{-1}	0.00891	0.01197	0.01690
$Al_2(SO_4)_3$	k/min^{-1}	0.01429	0.01767	0.02320
MgSO4	k/min^{-1}	0.01157	0.01492	0.01911
Na_2SO_4	k/min^{-1}	0.01210	0.01572	0.01978
K_2SO_4	k/min^{-1}	0.01231	0.01611	0.02070

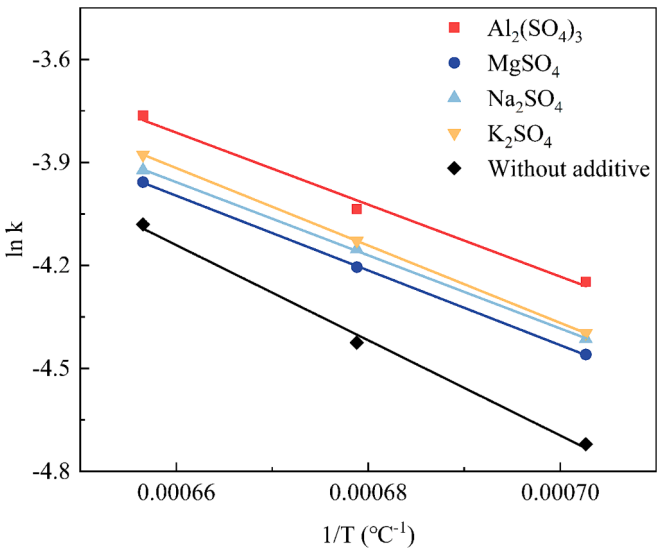

Fig. 12. The relationship between ln k and $1/T$ in phosphate rock reduction.

Table 9
The outcomes of fitting in various systems.

Additive	ln k/T	$E/\text{kJ·mol}^{-1}$	r^2
None	$\ln k = -13862.25/T + 5.01$	115.25	0.992
$Al_2(SO_4)_3$	$\ln k = -10480.58/T + 3.10$	87.14	0.983
$MgSO_4$	$\ln k = -10881.68/T + 3.18$	90.47	0.999
Na_2SO_4	$\ln k = -10654.40/T + 3.07$	88.58	0.999
K_2SO_4	$\ln k = -11273.47/T + 3.52$	93.73	0.999

Industrial feasibility analysis

Economic comparison of phosphorite reduction processes

In order to fully illustrate the feasibility and economic advantages of the fluidized bed phosphate reduction process, the main phosphorite reduction processes are compared by consulting the existing industrial equipment operation data and relevant literature [38,46,47–52]. The results are summarized in Table 10.

From Table 10, The equipment for wet phosphorite reduction is simple, but there are many by-products, and acid and wastewater treatment systems are required, which may increase hidden costs. The treatment of the by-product phosphogypsum is very difficult and requires high costs. Wet phosphoric acid must use high-grade phosphorite. China only has 7 % of high-grade phosphorite, and there are questions about whether it can be used sustainably. The blast furnace method relies on coal and large furnace bodies, and the initial investment is the

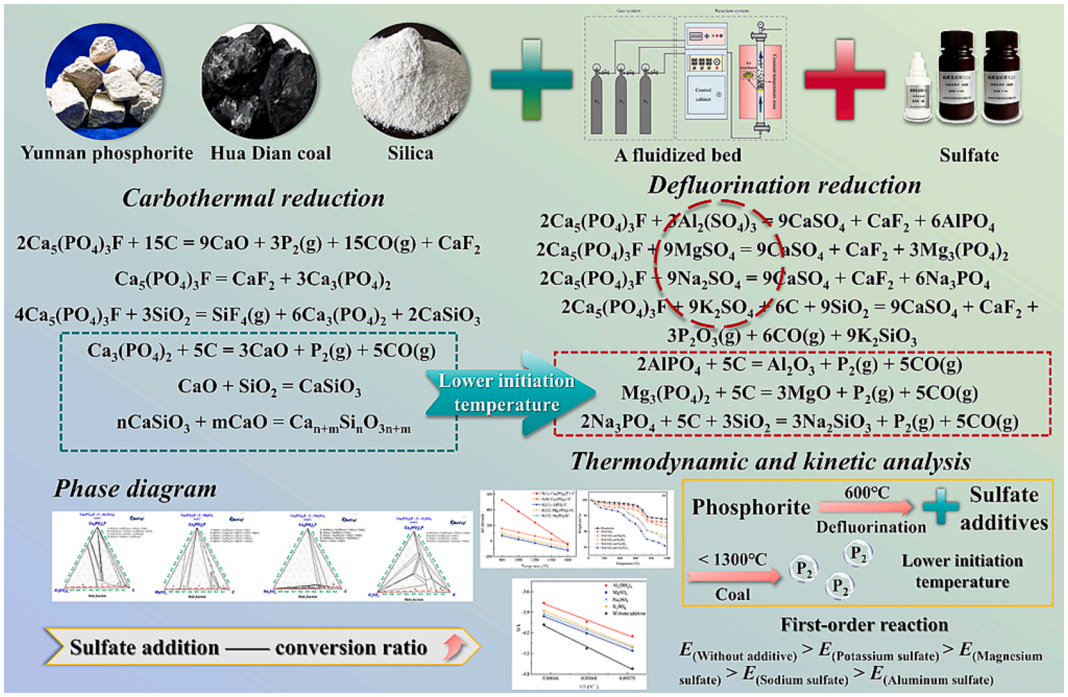

Fig. 13. Mechanism diagram of phosphorite reduction with sulfate additives in a fluidized bed.

Table 10
Comparison of the economic performance of the main existing phosphorite reduction processes.

Index	Fluidized bed	Kiln	Wet reduction	Blast furnace
Investment cost	Medium (low device complexity)	Higher (large demand for high temperature equipment)	Low (simple equipment)	High (large furnace and accessories)
Running costs	Low (low energy consumption)	High (high equipment maintenance cost)	Medium (water consumption and post-treatment)	Highest (low reduction rate)
Raw material utilization	65–85 %*	50–70 %	90–95 %(High acid consumption)	40–65 %(Large coal consumption)
Environmental costs	Low (high efficiency desulfurization, less solid waste)	Medium	High (wastewater and phosphogypsum treatment costs)	Highest (dust, exhaust gas)
By-product	Slag	Slag	Phosphogypsum, sulfuric acid (requires high cost for processing and separation)	High carbon content slag
Comprehensive cost ($GJ•t^{-1}$)	<1000*	1200–1500	1000–1200	1500–1800
Limitation	The reaction temperature should not be too high	Equipment is prone to corrosion and has high maintenance costs	The by-products are difficult to handle and the grade of the phosphorite is extremely high	Low utilization rate of phosphorite and high coal consumption

*: Predicted values based on existing data.

highest. In addition, it has the lowest utilization ratio of coal and phosphorite and is currently being gradually replaced. The kiln method will cause serious corrosion problems during industrial operation, and its large-scale industrial utilization is currently hindered. Fluidized bed thermal reduction of phosphorite can utilize existing fluidized bed equipment, which is significantly better than traditional processes in phosphorite applicability and raw material utilization. Especially under the background of the "Carbon peak and carbon neutrality" policy, its low energy consumption and high environmental compatibility can make it the core technical direction for the upgrading of phosphorus chemical industry. In the future, as large-scale fluidized bed technology matures (such as the promotion of thousand-ton equipment), its economic advantages will be further highlighted.

Feasibility analysis of phosphorite reduction in a fluidized bed

In order to make this study more applicable to industrial operation, based on the conclusions and data, this section will provide suggestions for scale-up experiments and industrial equipment. The material used for the fluidized bed furnace in this experiment is corundum tube. The reaction temperature range of the fluidized bed phosphorite reduction process is 1200–1300 ℃. Considering the high working temperature, the industrial operation device can use SiC-Al_2O_3 composite lining (thickness 150 mm), whose thermal shock stability at 1600 ℃ reaches 15 hot and cold cycles [53], which can ensure continuous and stable operation at high temperature. In terms of temperature control, the industrial operation device sets a double-layer annular hood in the feeding section, and cooperates with the fuzzy PID algorithm to reduce the bed temperature fluctuation to ± 8 ℃ [54,55]. In terms of temperature gradient control, a three-level temperature control zone is designed (preheating zone 900 ℃→reaction zone 1250 ℃→slow cooling zone 700 ℃). Meanwhile, accurate real-time data is measured and the operation of each component in the equipment is maintained to achieve precise adjustment of reaction temperature and gas flow, ensuring the stability and repeatability of the process. For the reactor scale-up and simulation, an industrial-grade reactor heat and mass transfer model can be established based on the Glicksman fluidized bed scale-up criterion [56] for

further optimization of the reactor. In terms of process optimization, industrial equipment can consider adding a soft measurement model based on LSTM neural network to build a "perception-prediction-control" three-in-one control system. Combined with infrared thermal imaging online monitoring, multivariable decoupling control of P_2 concentration-temperature–pressure can be achieved to predict the phosphorite reduction ratio in real time and adjust the process parameters in time.

Operational stability analysis

Unlike other thermal reduction processes for phosphorite, the issues of material wear and stable operation of the reactor need to be considered during the fluidized bed operation. During long-term operation of a fluidized bed reactor, particle wear may lead to a reduction in particle size. The average particle size of the particles after the reaction will be smaller than the initial 150 μm. Based on the Kunii-Levenspiel model [57], a reduction in particle size will improve gas diffusion efficiency, but the bed pressure drop needs to be monitored to ensure normal operation of the device. During industrial-scale fluidized bed operation, it is necessary to consider regular replenishment of fresh particles to maintain stable fluidization. During high-temperature reduction, silica and phosphorite may form a low-melting-point eutectic phase, resulting in slag deposition. Therefore, before large-scale operation, it is necessary to control risks by optimizing the feed rate and determining the slag removal cycle. Ordinary 310s stainless steel used as the inner wall of a fluidized bed reactor may corrode or be damaged by high temperature in a high-temperature environment. In order to extend the service life and ensure the stable operation of the fluidized bed, large-scale industrial equipment should use Al_2O_3 coating (plasma spraying) or use nickel-based alloys (such as Inconel 600) [58,59].

By-product analysis

This study will add sulfate waste to the reduction process of phosphorite. The proportion of silica in sulfate waste in industrial production is about 40–60 %, and the sulfate content is usually 5–10 %. Among them, sulfate will participate in the reduction reaction of phosphorite, and most of the sulfuric acid will react to form CaS and $CaSO_4$. These substances are relatively stable and will remain in the solid phase. The pilot experiment used a Gasmet portable Fourier transform infrared gas analyzer to measure the tail gas. The SO_x concentration in the tail gas was less than 10 ppm, which meets the 150 ppm limit of GB 16297-1996. The fluidized bed process can more effectively utilize coal and phosphorite resources. The carbon content in its ash is much lower than that of the blast furnace method, and it is rich in a large amount of calcium compounds. This can make the ash meet the application requirements of cement blending. Cement blending these ashes containing a large amount of calcium compounds can theoretically improve the strength of the material. During the phosphorite reduction process, the added sulfate may react with SiO_2 in the phosphorite at high temperature to form silicate. However, the intense mixing of gas and solid in the fluidized bed avoids excessive local contact between sulfate and SiO_2, which can effectively inhibit such side reactions. Although silicate will be generated in the process, the sulfate content itself is relatively low, so the generation is also relatively small. The small amount of silicate generated in the ash can further increase the hardness of cement when used for cement blending. Therefore, this process can make better use of by-products when used industrially, and the additional benefits of each ton of phosphate processing can be further increased.

Environmental and sustainability analysis

This study explored the feasibility of adding sulfate waste to the reduction process of phosphorite. In the industrial sulfate production, a large amount of waste containing silica and a small amount of sulfate is generated. These wastes will cause serious environmental pollution and have extremely high treatment costs. The effective use of these wastes is of great significance to industry. The "China Industrial Solid Waste Treatment White Paper 2023″ stipulates that the hazardous waste disposal fee is ￥1000-2000/t. This process can treat a large amount of sulfate waste, and the phosphorite slag can also be used as an admixture for cement industrial products such as Portland cement. This will greatly improve the economic benefits of the fluidized bed reduction of phosphorite process with the participation of sulfate waste. Moreover, silica originally needs to be added during the thermal reduction of phosphorite. The high content of silica and a small amount of sulfate in sulfate waste can not only improve the utilization ratio of phosphorite, but also save the cost of using silica. Therefore, compared with other current processes, the cost-effectiveness of this process has the most significant advantage in the whole life cycle.

Conclusions

This study explores the optimal circumstances for the carbothermal reaction of phosphorite using a bubbling fluidized bed reactor and investigates the promoting effect of sulfate on phosphorite reduction. This approach reduces the cost of thermal reduction process, and provides a method for recycling and disposing of hazardous sulfate industrial waste. The specific findings of the study are as follows.

(1) The best conditions of phosphorite reduction in a bubbling fluidized bed were explored, namely a $n_{(Si/Ca)}$ of 2.0–2.2, a carbon excess coefficient of 1.6, and 0.11 $m \bullet s^{-1}$ of the carrier gas.
(2) The introduction of sulfates has proven highly effective in enhancing the utilization of phosphorite. The optimal addition ratios for sulfate additives, aluminum sulfate, magnesium sulfate, potassium sulfate, and sodium sulfate, are found to be 12 %, 10 %, 3.5 %, and 4.5 %, respectively. Potassium sulfate exhibited the most pronounced promotion effect, increasing the conversion ratio from 58.43 % to 72.96 %.
(3) Pretreatment of phosphorite with these additives further improved the conversion ratio. Aluminum sulfate demonstrated the most significant effect, increasing the conversion ratio from 63.57 % without additives to 79.95 %.
(4) Kinetic analysis reveals that compared to the reaction system without additive, the addition of aluminum sulfate, magnesium sulfate, sodium sulfate, and potassium sulfate reduces the activation energy by 28.11 $kJ \cdot mol^{-1}$, 24.78 $kJ \cdot mol^{-1}$, 26.67 $kJ \cdot mol^{-1}$, and 21.52 $kJ \cdot mol^{-1}$, respectively.

CRediT authorship contribution statement

Zhihua Tian: Writing – original draft, Methodology, Formal analysis, Data curation. **Bin Zhang:** Writing – review & editing, Methodology. **Jiahe Yue:** Writing – review & editing, Visualization. **Qinhui Wang:** Writing – review & editing, Resources, Project administration, Methodology.

Funding

Thanks for the financial support by the Fundamental Research Funds for the Central Universities (2022ZFJH004).

Declaration of competing interest

The authors declare that they have no known competing financial interests or personal relationships that could have appeared to influence the work reported in this paper.

References

[1] C. James, L. Rachel, B. David, et al., The future distribution and production of global phosphate rock reserves [J], Resour. Conserv. Recycl. 57 (2011) 78–86.
[2] B. Ronghu, Phosphate price peaks and negotiations - Part 1: Fundamentals and the 1975 peak[J], Resour. Policy 83 (2023) 103587.

[3] J.A.W. Paul, J.E. James, H. Julian, et al., Greening the global phosphorus cycle: How green chemistry can help achieve planetary P sustainability[J], Green Chem. 4 (2015) 2087–2900.
[4] L. Reijnders, Phosphorus resources, their depletion and conservation, a review[J], Resource, Conservation & Recycling 93 (2014) 32–49.
[5] A. Abouzeid, Physical and thermal treatment of phosphate ores - An overview[J], Int. J. Miner. Process. 85 (4) (2008) 59–84.
[6] K. Ye, H. Li, K. Luo, et al., Removal of fluorine, sulfur and arsenic from wet-process phosphoric acid[J], Sci. & Technol. in Chem. Industry 25 (4) (2017) 59–64.
[7] W. Yang, B. He, G. Zhu, et al., Review on the technology of wet-process phosphoric acid from phosphate rock[J], Phosphate & Compound Fertilizer 37 (8) (2022) 26–28.
[8] H. Jing, Y. Yao, C. Hou, et al., Effects of K_2O addition on the reduction smelting of phosphorite for the yellow phosphorus production[J], Characterization of Minerals, Metals, and Mater. 17 (2021) 373–382.
[9] Q. Yang, S. Yang, C. Ma, et al., Effect of pretreatment on phosphate smelting reduction reaction[J], Industrial Minerals & Processing 45 (12) (2016) 3–5.
[10] R. Cao, J. Xia, W. Li, et al., Effects of alkali metal carbonates on carbothermal reduction of phosphate rock[J], J. Chem. Eng. Chin. Univ. 32 (3) (2018) 568–576.
[11] W. Yan, L. Li, R. Huang, et al., Thermodynamic simulation study on reducing mid-low-grade phosphorite by carbothermic reduction in vacuum[J], Guangzhou Chem. Industry 45 (12) (2017), 101–103+164.
[12] B. Lei, Y. Mei, Y. Yang, et al., Developmental trend on the technique of thermal-process phosphoric Acid[J], Yunnan Chem. Industry 06 (2007) 64–68.
[13] Y. Mei, Y. Yang, Y. Song, et al., The heat recovery and utilization in the production of furnace-process phosphoric acid[J], Strategic Study of CAE 1 (2005) 347–353.
[14] Y. Mei, Energy saving and emission reduction, circular economy is the road to development of thermal basic phosphorus processing[J], Phosphate & Compound Fertilizer 31 (7) (2016) 12.
[15] J. Jiang, Way for the development and utilization of low-grade phosphate rock[J], Multipurpose Utilization of Mineral Resources 4 (2014) 16–19.
[16] Y. Li, Z. Chen, Y. Jin, et al., Study of the Silica or K-feldspar as fluxing agent for the yellow phosphorus production[J], Phosphorus Sulfur Silicon Relat. Elem. 193 (8) (2018) 1–29.
[17] Y. Mei, L. Fan, X. Liang, et al., Technoeconomic analusis on phosphoric acid by furnace process and phosphoric acid by wet process[J], Inorganic Chem. Industry 43 (01) (2011) 4–7.
[18] X. Wang, L. Tang, Z. Jiang, Numerical simulation of venturi ejector reactor in yellow phosphorus purification system[J], Nuclear Engineer & Design 268 (3) (2014) 18–23.
[19] X. Li, B. Hu, Y. Wu, et al., Process parameters and kinetics of smelting reduction technology for low-grade phosphate ore reduction[J], J. Chem. Eng. Chin. Univ. 28 (4) (2014) 905–910.
[20] G. Jiang. Study on the Phosphorus Volatile in the Process of Pyrolyzing the Middle and Low-grade Phosphate Rock [D]. Zhengzhou University, 2013.
[21] B. Hu, Study on process optimization and mechanism of phosphate ore smelting reduction[D], Wuhan Institute of Technol. (2014).
[22] F. Lan. Study on the Melting Characteristics of Phosphate Rock with Addition of Silicon-Aluminum-Magnesium Oxide Flux [D]. Zhengzhou University, 2016.
[23] B. Luo, Study on optimization of carbothermal reduction process for medium-low grade phosphate rock[D], Wuhan Institute of Technol. (2020).
[24] K.C. Biswal, T. Bhowmik, G.K. Roy, Prediction of pressure drop for a conical fixed bed of spherical particles in gas—solid systems[J], The Chem. Eng. J. 29 (1) (1984) 47–50.
[25] D.C. Sau, S. Mohanty, K.C. Biswal, Prediction of critical fluidization velocity and maximum bed pressure drop for binary mixture of regular particles in gas–solid tapered fluidized beds[J], Chem. Eng. Process. 47 (12) (2008) 2114–2120.
[26] K.C. Biswal, T. Bhowmik, G.K. Roy, Prediction of minimum fluidization velocity for gas-solid fluidization of regular particles in conical vessels[J], The Chem. Eng. J. 30 (1) (1985) 57–62.
[27] H. Xu, W. Wang, W. Zhong, et al., Experimental study of fluidization characteristics of Geldart-D particles in pressurized bubbling fluidized bed[J], Adv. Powder Technol. 33 (3) (2022) 103453.
[28] Q. Guo, Y. Xu, X. Yue, Fluidization characteristics in micro-fluidized beds of various inner diameters[J], Chem. Eng. Technol. 32 (12) (2009) 1992–1999.
[29] G. Kresse, J. Furthmüller, Efficiency of ab-initio total energy calculations for metals and semiconductors using a plane-wave basis set[J], Phys. Rev. B 6 (1996) 15–50.
[30] G. Kresse, J. Furthmüller, Efficient Iterative Schemes for Ab Initio Total-Energy Calculations Using a Plane-Wave Basis Set[j]. 54 (1996) 11169–11186.
[31] J.P. Perdew, M. Ernzerhof, K. Burke, Rationale for mixing exact exchange with density functional approximations[J], J. Chem. Phys. 1996 (105) (1996) 9982–9985.
[32] S. Grimme, J. Comput, Semiempirical GGA-type density functional constructed with a long-range dispersion correction[j]. J. Compytational Chem. 27 (2006) 1787–1799.
[33] J.K. Christie, R.I. Ainsworth, N.H. de Leeuw, Ab initio molecular dynamics simulations of structural changes associated with the incorporation of fluorine in bioactive phosphate glasses[J], Biomaterials 35 (24) (2014) 6164–6171.
[34] Y. Zhao, J. Xia, R. Cao, Feasibility study on potassium additive promoting carbothermal reduction of phosphate rocks[J], Bulletin of the Chinese Ceramic Soc. 37 (12) (2018) 3983–3988.
[35] X. Li, Z. Hu, Y. Liu, et al., Study on reduction of low grade phosphorite in Yunnan by kiln process[J], Phosphate & Compound Fertilizer 31 (2) (2016) 11–12.
[36] B. Hu, C. Ma, K. Gui, et al., Effect of inorganic additives on smelting reduction of phosphate rock[J], Industrial Minerals & Process. 43 (6) (2014), 1–2+8.
[37] Y. He, H. Zheng, L. Lv, et al., Carbothermal reduction process of low-grade mixed phosphate ore[J], Inorganic Chem. Industry 53 (11) (2021) 95–99.
[38] M. Li, C. Ye, S. Li, et al., Current status and research progress of thermal reduction technology for producing yellow phosphorus from phosphate rock[J], Chem. Industry and Eng. Progress 43 (7) (2024) 3578–3592.
[39] Y. Li, J. Xia, H. Liu, et al., Mechanism of silica and K-feldspar as flux agents in phosphate ore carbothermic reduction[J], J. Chem. Eng. Chin. Univ. 31 (5) (2017) 1120–1126.
[40] X. Li, Q. Wu, X. Lv, et al., Effect of SiO_2/CaO ratio on thermal carbon reduction of low-grade phosphate ore in low vacuum[J], Chin. J. Vac. Sci. Technol. 41 (7) (2021) 687–693.
[41] X. Cheng, J. Pang, L. Luo, et al., Analytical study of non-isothermal kinetics of phosphorus extraction by silica thermal process[J], Multipurpose Utilization of Mineral Resources 12 (2024) 1–10.
[42] J. Yang, J. Chen, H. Liu, et al., Enhanced effect of aluminum impurity on solid state carbothermal reduction of fluorapatite[J], J. Sichuan Univ. Eng. (science Edition) 47 (1) (2015) 186–191.
[43] Q. Li, B. Hu, Y. Wu, et al., Reaction kinetics of phosphate ore with carbonby smelting reduction technology[J], Chem. Eng. of China 41 (4) (2013) 53–56.
[44] E.J.K. Nilsson, M.S. Johnson, O.J. Nielsen, et al., Kinetics of the gas-phase reactions of chlorine atoms with CH_2F_2, CH_3CCl_3, and CF_3CFH_2 over the temperature range 253-553 K[J], Int. J. Chem. Kinet. 41 (6) (2009) 401–406.
[45] C.A. Cuevas, A. Notario, E. Martínez, et al., Influence of temperature in the kinetics of the gas-phase reactions of a series of acetates with Cl atoms[J], Atmos. Environ. 39 (28) (2009) 5091–5099.
[46] S. Liu, Analysis of the substitution effect of wet-process purified phosphoric acid on thermal-process phosphoric acid[J], Eco-Industry Sci. & Phosphorus Fluorine Eng. 39 (7) (2024) 33–37.
[47] Y. Qi, S. Zhang, New research progress and present application situation of purification technology for wet-process phosphoric acid[J], Appl. Chem. Industry 51 (9) (2022) 2798–2804.
[48] Y. Mei, Energy saving and emission reduction, circular economy is the road to the development of thermal basic phosphorus processing[J], Phosphate & Compound Fertilizer 31 (7) (2016) 2.
[49] Y. Yao, H. Jing, Y. Yin, et al., Research status and suggestions of yellow hosphorus production technology by thermal processing under peak carbon dioxide emission and carbon neutrality[J], Chem. Industry and Eng. Progress 43 (3) (2024) 2104–2116.
[50] A. Chen, J. Zhu, K. Chen, et al., Melt suspension crystallization for purification of phosphoric acid[J], Asia Pac. J. Chem. Eng. 8 (2012) 354–361.
[51] B. Zhong, W. Fang, J. Li, et al., Progress in purification technology (engineering) of wet process phosphoric acid in China[J], Inorganic Chem. Industry 45 (2) (2013) 8–10.
[52] L. Dou, F. Yang, J. Qu, Development process of blast furnace phosphorus refining and its prospects[J], Shanxi Chem. Industry 11 (4) (1991) 29–31.
[53] I. Ahmed, M. Duchesne, Y. Tan, et al., Electrically heated fluidized beds—A review [J], Ind. Eng. Chem. Res. 63 (10) (2024) 4205–4235.
[54] B. Chen, Q. Xie, J. Zhou, Fuzzy adaptive PID control of biomass circulating fluidized bed boiler[J], Chinese Automation Congress (2018) 3795–3800.
[55] L. Reznik, O. Ghanayem, A. Bourmistrov, PID plus fuzzy controller structures as a design base for industrial applications[J], Eng. Appl. Artif. Intel. 13 (4) (2000) 419–430.
[56] L.R. Glicksman, Scaling relationships for fluidized beds[J], Chem. Eng. Sci. 39 (9) (1984) 1373–1379.
[57] D. Kunii, O. Levenspiel, Fluidization engineering (Second Edition) [M], Butterworth-Heinemann, 1991.
[58] S. Zhang, H. Li, Z. Jiang, et al., Chloride- and sulphate-induced hot corrosion mechanism of super austenitic stainless steel S31254 under dry gas environment [J], Corros. Sci. 163 (2020) 108295.
[59] S.R. Pillai, High temperature corrosion of austenitic stainless steels[J], Corrosion of Austenitic Stainless Steels (2002) 265–286.